UC Davis
UC Davis Previously Published Works

Title

Haploinsufficiency of NFKBIA reshapes the epigenome antipodal to the IDH mutation and imparts disease fate in diffuse gliomas

Permalink

https://escholarship.org/uc/item/8cw4j553

Journal

Cell Reports Medicine, 4(6)

ISSN

2666-3791

Authors

Bredel, Markus

Espinosa, Lluís

Kim, Hyunsoo

et al.

Publication Date
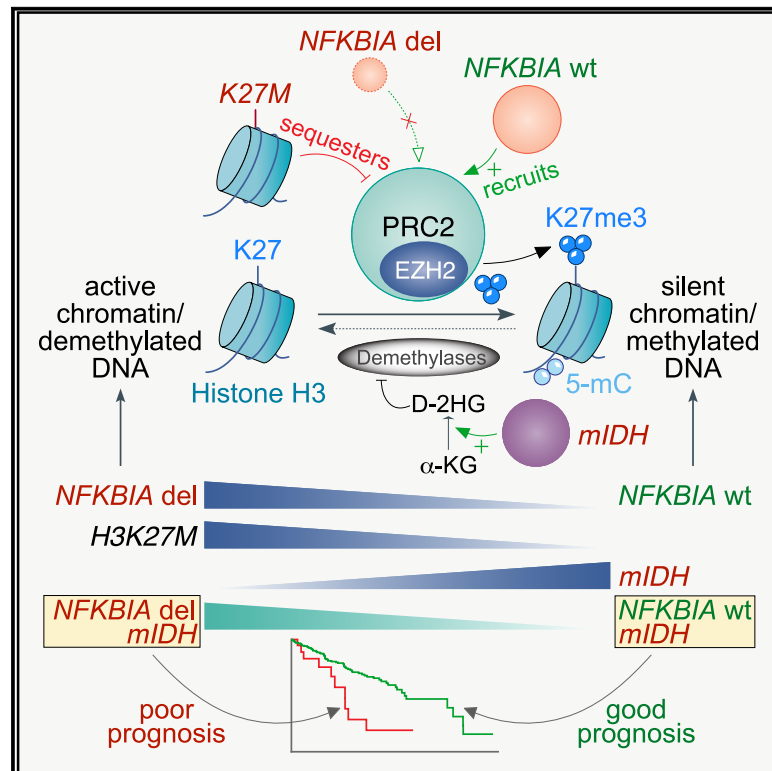
2023-06-01

DOI

10.1016/j.xcrm.2023.101082

Peer reviewed

Article

Haploinsufficiency of *NFKBIA* reshapes the epigenome antipodal to the *IDH* mutation and imparts disease fate in diffuse gliomas

Graphical abstract

Authors

Markus Bredel, Lluís Espinosa, Hyunsoo Kim, ..., David R. MacDonald, Stephanie L. Pugh, Arnab Chakravarti

Correspondence

mbredel@uab.edu

In brief

Bredel et al. characterize multiple adult diffuse glioma populations and reveal that haploinsufficient deletions of *NFKBIA* portend poor patient prognosis and align with epigenome and transcriptome landscapes that are antithetical to those induced by the *IDH* mutation and partly reminiscent of those induced by the *H3K27M* mutation in pediatric gliomas.

Highlights

- *NFKBIA* deletions exhibit a distinct pattern relative to other key genetic markers

- *NFKBIA* deletions reshape the DNA and histone methylome antipodal to the *IDH* mutation

- *NFKBIA* deletions engender a transcriptome landscape reminiscent of *H3K27M* mutant glioma

- *NFKBIA* deletions independently portend poor patient prognosis

CellPress

Cell Reports Medicine

Article

Haploinsufficiency of *NFKBIA* reshapes the epigenome antipodal to the *IDH* mutation and imparts disease fate in diffuse gliomas

Markus Bredel,[1,26,*] Lluís Espinosa,[2] Hyunsoo Kim,[3] Denise M. Scholtens,[4] Joseph P. McElroy,[5] Rajani Rajbhandari,[1] Wei Meng,[6] Thomas M. Kollmeyer,[7] Tathiane M. Malta,[8] Michael A. Quezada,[9] Griffith R. Harsh,[10] Teresa Lobo-Jarne,[2] Laura Solé,[2] Aran Merati,[1] Surya Nagaraja,[9] Sindhu Nair,[1] Jaclyn J. White,[11] Nanda K. Thudi,[1] Jessica L. Fleming,[6]

(Author list continued on next page)

[1]Department of Radiation Oncology, O'Neal Comprehensive Cancer Center, The University of Alabama at Birmingham Heersink School of Medicine, Birmingham, AL 35294, USA
[2]Cancer Research Program, Centro de Investigación Biomédica en Red Cáncer (CIBERONC), Institut Mar d'Investigacions Mèdiques, Hospital del Mar, 08003 Barcelona, Spain
[3]Lineberger Comprehensive Cancer Center, University of North Carolina at Chapel Hill, Chapel Hill, NC 27599, USA
[4]Division of Biostatistics—Department of Preventive Medicine, Northwestern University Feinberg School of Medicine, Chicago, IL 60611, USA
[5]Center for Biostatistics—Department of Biomedical Informatics, James Cancer Hospital and Solove Research Institute, The Ohio State University College of Medicine, Columbus, OH 43210, USA
[6]Department of Radiation Oncology, James Cancer Hospital and Solove Research Institute, The Ohio State University College of Medicine, Columbus, OH 43210, USA
[7]Department of Laboratory Medicine and Pathology, Mayo Clinic, Rochester, MN 55905, USA
[8]Department of Neurosurgery, Hermelin Brain Tumor Center, Henry Ford Health System, Detroit, MI 48202, USA
[9]Department of Neurology & Neurological Sciences and Howard Hughes Medical Institute, Stanford University School of Medicine, Stanford, CA 94305, USA
[10]Department of Neurological Surgery, University of California at Davis School of Medicine, Sacramento, CA 95817, USA
[11]Department of Neurosurgery, Wake Forest University School of Medicine, Winston-Salem, NC 27103, USA
[12]Department of Neurosurgery, Nagoya University School of Medicine, Nagoya 464-8601, Japan
[13]Department of Pathology and Tumor Biology, Kyoto University, Kyoto 606-8501, Japan
[14]Institute for Human Genetics, Hannover Medical School, 30625 Hannover, Germany

(Affiliations continued on next page)

SUMMARY

Genetic alterations help predict the clinical behavior of diffuse gliomas, but some variability remains uncorrelated. Here, we demonstrate that haploinsufficient deletions of chromatin-bound tumor suppressor NFKB inhibitor alpha (*NFKBIA*) display distinct patterns of occurrence in relation to other genetic markers and are disproportionately present at recurrence. *NFKBIA* haploinsufficiency is associated with unfavorable patient outcomes, independent of genetic and clinicopathologic predictors. *NFKBIA* deletions reshape the DNA and histone methylome antipodal to the *IDH* mutation and induce a transcriptome landscape partly reminiscent of *H3K27M* mutant pediatric gliomas. In *IDH* mutant gliomas, *NFKBIA* deletions are common in tumors with a clinical course similar to that of *IDH* wild-type tumors. An externally validated nomogram model for estimating individual patient survival in *IDH* mutant gliomas confirms that *NFKBIA* deletions predict comparatively brief survival. Thus, *NFKBIA* haploinsufficiency aligns with distinct epigenome changes, portends a poor prognosis, and should be incorporated into models predicting the disease fate of diffuse gliomas.

INTRODUCTION

Gliomas are the most frequently occurring primary brain tumors. Comprehensive genome-wide characterization has illuminated their molecular complexity.[1–7] Among their key genetic alterations identified, mutations of isocitrate dehydrogenase 1 (*IDH1*) and 2 (*IDH2*) genes (collectively referred to as *IDH*),[8] mutations in the promoter of telomerase reverse transcriptase

(*TERT*) and ATRX chromatin remodeler (*ATRX*) genes,[9,10] and codeletion of chromosome arms 1p and 19q (1p19q codeletion)[11] are associated with glioma subsets possessing distinct clinical trajectories.[1] Moreover, homozygous deletion of cyclin-dependent kinase inhibitor 2A/B (*CDKN2A/B*) is a biomarker of grade and prognosis, especially in *IDH* mutant gliomas.[12] These alterations are currently the most potent genetic markers predicting glioma aggressiveness.[1] *IDH* mutations manifest the

Amy Webb,[5] Atsushi Natsume,[12] Seishi Ogawa,[13] Ruthild G. Weber,[14] Joan Bertran,[15] S. Jaharul Haque,[6]
Bettina Hentschel,[16] C. Ryan Miller,[17] Frank B. Furnari,[18] Timothy A. Chan,[19] Anca-Ligia Grosu,[20] Michael Weller,[21]
Jill S. Barnholtz-Sloan,[22] Michelle Monje,[9] Houtan Noushmehr,[8] Robert B. Jenkins,[7] C. Leland Rogers,[23]
David R. MacDonald,[24] Stephanie L. Pugh,[25] and Arnab Chakravarti[6]

[15]Biosciences Department, Faculty of Sciences, Technology, and Engineering. University of Vic-Central University of Catalonia, 08500 Vic, Spain
[16]Institute for Medical Informatics, Statistics and Epidemiology, University of Leipzig, 04107 Leipzig, Germany
[17]Division of Neuropathology—Department of Pathology, O'Neal Comprehensive Cancer Center, The University of Alabama at Birmingham Heersink School of Medicine, Birmingham, AL 35294, USA
[18]Laboratory of Tumor Biology, Division of Regenerative Medicine—Department of Medicine, University of California at San Diego, La Jolla, CA 92093, USA
[19]Center for Immunotherapy and Precision Immuno-Oncology, Lerner Research Institute, Cleveland Clinic, Cleveland, OH 44195, USA
[20]Department of Radiation Oncology, Comprehensive Cancer Center, University of Freiburg, 79106 Freiburg, Germany
[21]Department of Neurology, University Hospital and University of Zurich, 8091 Zurich, Switzerland
[22]Division of Cancer Epidemiology and Genetics—National Cancer Institute, National Institutes of Health, Bethesda, MD 20892, USA
[23]Gamma West Cancer Services, Salt Lake City, UT 84124, USA
[24]London Regional Cancer Program, Western University, London, ON N6A 5W9, Canada
[25]NRG Oncology Statistics and Data Management Center, Philadelphia, PA 19103, USA
[26]Lead contact
*Correspondence: mbredel@uab.edu
https://doi.org/10.1016/j.xcrm.2023.101082

epigenetic glioma cytosine-phosphate-guanine (CpG) island methylator phenotype (G-CIMP),[13] which portends a favorable prognosis,[14,15] as does high vs. low G-CIMP.[4,16] Mutations (lysine-to-methionine substitution) in histone H3 (*H3K27M*)—involving the *H3F3A* locus of histone variant H3.3 and the *HIST1H3B* locus in the H3.1 or H3.2 variants[17]—characterize a subgroup of aggressive diffuse midline gliomas in children and young adults.[18,19] *H3K27M* mutant oncohistone induces a dose-dependent inhibition of the H3K27me3 methyltransferase complex, polycomb repressive complex 2 (PRC2).[20,21] PRC2 orchestrates genome architecture and mediates silencing of developmental genes during lineage specification and commitment.[22]

The NFKB inhibitor alpha (*NFKBIA*) gene at 14q13.2 encodes the alpha subunit of the inhibitors of κB (IκBα), proteins that regulate the activity of transcription factor nuclear factor κB (NF-κB) in the cytoplasm.[23] Evidence that, in chromatin, nuclear NFKBIA dynamically interacts with histones H2A and H4 to regulate polycomb-dependent transcriptional repression and, thus, stem cell maturation, lineage specification, and cancer[24–26] and our characterization of *NFKBIA* as a tumor suppressor in glioblastoma[27] prompted our investigation of the relationship of *NFKBIA* deletions with other genetic markers, alterations in the methylome, and the clinical course of gliomas. We analyzed the genetic profiles of gliomas of multiple well-characterized patient populations to determine whether incorporation of *NFKBIA* deletions could enhance the prognostic value of current molecular descriptions.[1,4]

RESULTS

Overview of patient population characteristics
We analyzed 2,255 patients and their 2,343 diffuse gliomas. The demographic and disease characteristics of patients of seven glioma populations are summarized in Table S1, and their clinicopathologic-genetic details are listed in Table S2. We used population 1 to test the relationship between *NFKBIA* deletions and key genetic alterations and survival in lower-grade (World

Health Organization [WHO] grade 2–3) gliomas and populations 2 and 3 for validation; population 4 to test the relationship of *NFKBIA* with key genetic alterations and survival in WHO grade 2–4 gliomas and population 5 for validation; population 6 to assess the relationship between *NFKBIA* deletion and tumor recurrence; and population 7 to study the intersection of gene signatures associated with *NFKBIA* deleted gliomas and *H3K27M* mutant diffuse intrinsic pontine gliomas (DIPGs).
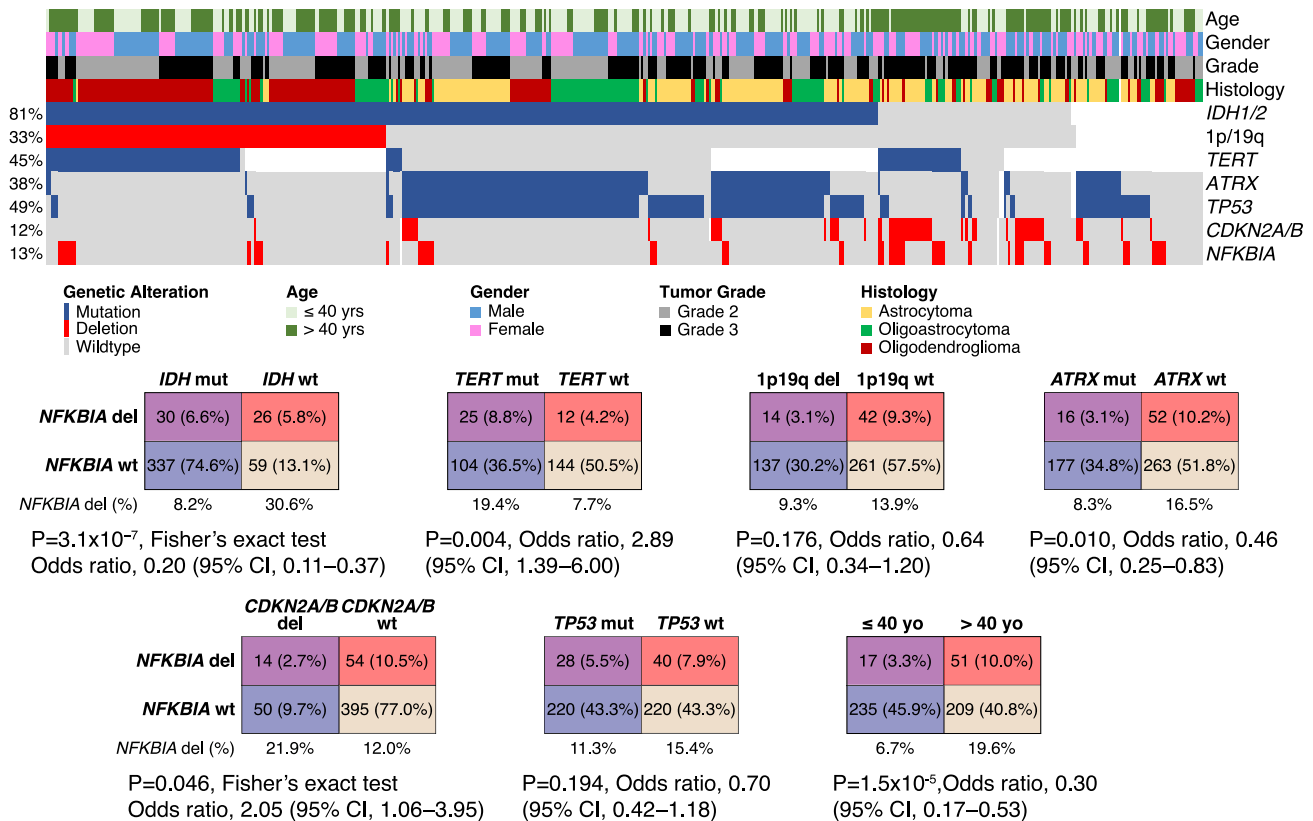
Deletion of *NFKBIA* in lower-grade gliomas
We observed a common hemizygous deletion encompassing *NFKBIA* in 68 of 513 (13.3%) lower-grade gliomas in population 1 (Figure 1A). *NFKBIA* deletions ranged from small (12.3 kbp) losses involving only the *NFKBIA* locus (chr14: 35,401,079–35,404,749) to larger chromosomal regions encompassing *NFKBIA* (median: 36.6 Mbp, interquartile range: 43.5 Mbp), to those extending to the 14q terminus. In the three main genetic groups of adult lower-grade gliomas—*IDH* mutant/1p19q codeleted/*TERT* mutant, *IDH* mutant/1p19q non-codeleted/*ATRX* mutant, and *IDH* wild-type/*TERT* mutant—we found no predilection for either *IDH* mutant group (9.3% and 6.7%, respectively) but did find higher presence in the *IDH* wild-type group (30.6%) (Figure 1A). *NFKBIA* deletions occurred in 4 of 87 (4.6%) WHO grade 2 gliomas of population 2 and in 60 of 694 (8.6%) lower-grade gliomas of population 3.

Sequencing analysis showed that *NFKBIA* is rarely mutated in lower-grade gliomas. Only 3 of 508 (0.6%) tumors of population 1 harbored a total of four missense mutations and one truncating mutation in the coding region of *NFKBIA* (Figure 1B). Expression of all six *NFKBIA* exons in tumors in which *NFKBIA* was deleted was significantly lower than in tumors with two intact copies of *NFKBIA* (Figures 1B and 1C).
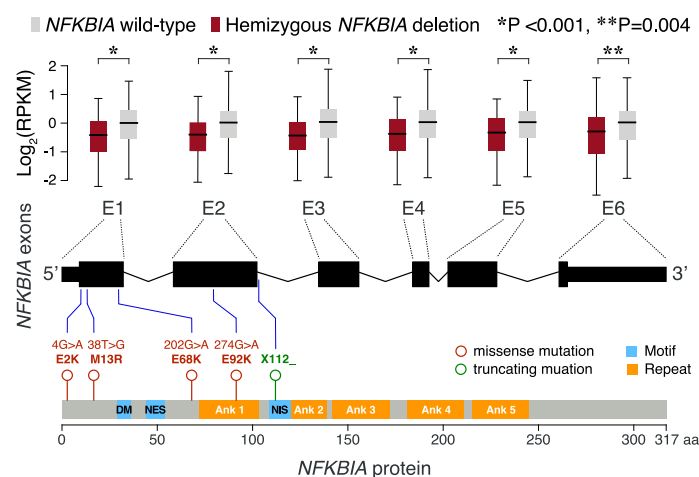
NFKBIA and key driver mutations in lower-grade gliomas
We sought to define the relationship between *NFKBIA* deletion and *IDH*, *TERT*, *ATRX*, and tumor protein P53 (*TP53*) mutations, 1p19q codeletions, and *CDKN2A/B* deletions, major early

A 516 WHO Grade 2–3 Gliomas in Population 1

	IDH mut	IDH wt
NFKBIA del	30 (6.6%)	26 (5.8%)
NFKBIA wt	337 (74.6%)	59 (13.1%)
NFKBIA del (%)	8.2%	30.6%

P=3.1x10⁻⁷, Fisher's exact test
Odds ratio, 0.20 (95% CI, 0.11–0.37)

	TERT mut	TERT wt
NFKBIA del	25 (8.8%)	12 (4.2%)
NFKBIA wt	104 (36.5%)	144 (50.5%)
NFKBIA del (%)	19.4%	7.7%

P=0.004, Odds ratio, 2.89
(95% CI, 1.39–6.00)

	1p19q del	1p19q wt
NFKBIA del	14 (3.1%)	42 (9.3%)
NFKBIA wt	137 (30.2%)	261 (57.5%)
NFKBIA del (%)	9.3%	13.9%

P=0.176, Odds ratio, 0.64
(95% CI, 0.34–1.20)

	ATRX mut	ATRX wt
NFKBIA del	16 (3.1%)	52 (10.2%)
NFKBIA wt	177 (34.8%)	263 (51.8%)
NFKBIA del (%)	8.3%	16.5%

P=0.010, Odds ratio, 0.46
(95% CI, 0.25–0.83)

	CDKN2A/B del	CDKN2A/B wt
NFKBIA del	14 (2.7%)	54 (10.5%)
NFKBIA wt	50 (9.7%)	395 (77.0%)
NFKBIA del (%)	21.9%	12.0%

P=0.046, Fisher's exact test
Odds ratio, 2.05 (95% CI, 1.06–3.95)

	TP53 mut	TP53 wt
NFKBIA del	28 (5.5%)	40 (7.9%)
NFKBIA wt	220 (43.3%)	220 (43.3%)
NFKBIA del (%)	11.3%	15.4%

P=0.194, Odds ratio, 0.70
(95% CI, 0.42–1.18)

	≤ 40 yo	> 40 yo
NFKBIA del	17 (3.3%)	51 (10.0%)
NFKBIA wt	235 (45.9%)	209 (40.8%)
NFKBIA del (%)	6.7%	19.6%

P=1.5x10⁻⁵, Odds ratio, 0.30
(95% CI, 0.17–0.53)

B 513 WHO Grade 2–3 Gliomas in Population 1

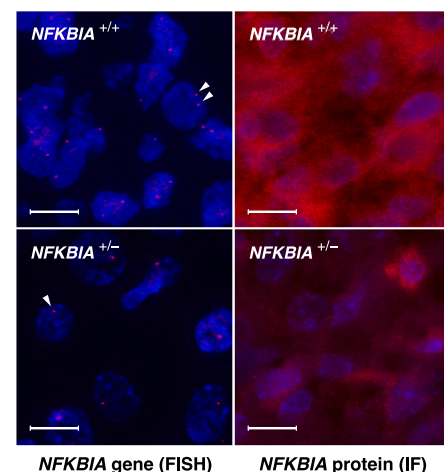**C** Glioma with or without NFKBIA deletion

Figure 1. NFKBIA deletions and expression in lower-grade gliomas

(A) Heatmap and two-way contingency tables showing the relationship between *NFKBIA* deletions and genetic alterations—*IDH*, *TERT*, *ATRX*, and *TP53* mutations, 1p19q codeletions, and *CDKN2A/B* deletions—and clinicopathologic variables in 516 lower-grade gliomas of population 1. OR, odds ratio; CI, confidence interval.

(B) Expression of the six *NFKBIA* exons—in log₂-transformed RPKM (reads per kilobase of exon model per million mapped reads)—in 513 *NFKBIA* deleted vs. wild-type lower-grade gliomas of population 1. Five rare missense or truncating mutations are mapped in relation to the exons and various *NFKBIA* protein motifs (DM, destruction motif; NES, nuclear export signal; NIS, nuclear import signal) and ankyrin (Ank) repeats. Error bars represent ±standard deviation. Wilcoxon rank-sum test.

(C) NFKBIA protein expression—by immunofluorescence (IF)—in two glioma samples with (+/−) and without (+/+) hemizygous *NFKBIA* deletion—by fluorescence *in situ* hybridization (FISH), indicating a haploinsufficiency effect. Red dots (arrowheads) represent one *NFKBIA* allele. Scale bars, 20 μm.

molecular alterations strongly associated with overall survival in lower-grade gliomas.[1,12] We observed distinct patterns of occurrence between *NFKBIA* deletion and the *IDH*, *TERT*, and *ATRX* mutations and between *NFKBIA* and *CDKN2A/B* deletions but no relationship with *TP53* mutations or 1p19q codeletions in population 1 (Figure 1A). We observed similar patterns between *NFKBIA* deletions and *IDH* mutations in population 2 and between *NFKBIA* deletions and *IDH* and *TERT* mutations in population 3 (Figure S1). We also noted an association of *NFKBIA* deletions with patient age in population 1 and population 3—patients older than 40 had a higher deletion frequency—but not in population 2 (Figures 1A and S1).

NFKBIA deletions and survival in patients with lower-grade gliomas

Association between *NFKBIA* deletions and survival was established in three groups of patients with newly diagnosed lower-grade glioma. Patients in population 1 with *NFKBIA* deleted tumors had shorter median survival (4.3 vs. 8.0 years) than those with non-deleted tumors (Figure 2A). Cox proportional-hazards regression confirmed that patients with *NFKBIA* deleted tumors had briefer survival (Figure S2A). An adjusted Cox model suggested that this association was independent of prognostic covariates, including *IDH*, *TERT*, *ATRX*, and *TP53* mutations, 1p19q codeletions, *CDKN2A/B* deletions, WHO grade, tumor histology, and patient age (Figure S2A). *NFKBIA* deletion also portended shorter recurrence-free survival (median 3.2 vs. 6.0 years) in population 1 (Figure 2B).

Similarly, mRNA expression data of population 1 showed association between *NFKBIA* expression and duration of overall survival when expression was dichotomized at the median. Association between *NFKBIA* expression and survival held in an adjusted Cox model that included the *IDH* mutation and other genetic and clinicopathologic variables (Figure S3).

We validated the relationship between *NFKBIA* deletions in low-grade (WHO grade 2) glioma patients of NRG Oncology/RTOG 9802 (population 2) and both overall survival and recurrence-free survival (Figures 2C and 2D). Median overall and recurrence-free survival for deleted vs. non-deleted tumors was 1.0 vs. 11.4 years and 0.7 vs. 5.1 years, respectively. Lest the smaller overall sample size and low variant frequency for *NFKBIA* deletion in population 2 inflate variance estimates, we included only the most relevant pathogenetic variables in an adjusted model. *NFKBIA* deletion remained independently associated with overall survival after adjusting for *IDH* mutation, 1p19q codeletion, and patient age (Figure S2B). As reported, patients who received both chemotherapy and radiation therapy survived longer than those who received radiation therapy alone.[28] In an adjusted Cox model, *NFKBIA* was associated with survival independent of treatment randomization (Figure S2B).

We also observed a significant relationship between *NFKBIA* and survival in the lower-grade gliomas of population 3 (Figure 2E). Because low variant frequency and some collinearity (e.g., between *IDH* and *ATRX* mutations and patient age) precluded modeling all available genetic and clinicopathologic predictors for population 3 in one statistical model, we developed separate clinicopathologic and genetic models, both of which

showed that *NFKBIA* deletions were independently associated with overall survival duration (Figure S2C).

Deletion of *NFKBIA* in WHO grade 2–4 diffuse gliomas

Molecular genetic alterations are used to predict the clinical behavior, response to therapy, and outcome of diffuse gliomas irrespective of glioma grade and histology.[1,2,4,12] We therefore examined the occurrence of *NFKBIA* deletions in WHO grade 2–4 gliomas relative to these alterations (Figure 3A). Among diffuse gliomas of population 4, we observed a patterned occurrence between *NFKBIA* deletions and *IDH*, *ATRX*, *TERT*, and *PTEN* mutations, 1p19q codeletions, *CDKN2A/B* deletions, and chromosome 7 gain/10 loss, but not with *TP53* mutations or *EGFR* amplifications (Figure 3A).

In two-class models of population 4 and population 5 patients stratified by *NFKBIA* deletion status, those with *NFKBIA* deleted tumors had briefer overall survivals (Figures 3B and 3C). Median survival times for tumors with and without *NFKBIA* deletions were 1.3 and 2.2 years in population 4 and 1.5 and 7.7 years in population 5, respectively. Adjusted Cox models revealed that the association between *NFKBIA* status and duration of overall survival was independent of covariates *IDH*, *TERT*, *ATRX*, *TP53*, and *PTEN* mutations, 1p19q codeletion, *CDKN2A/B* deletion, chromosome 7 gain/10 loss, *EGFR* amplification, WHO grade, tumor histology, patient age, and patient gender in population 4 and of available covariates *IDH*, *TERT*, and *ATRX* mutations, 1p19q codeletion, WHO grade, tumor histology, patient age, and patient gender in population 5 (Figures 3B and 3C). On subgroup analysis, the survival association of *NFKBIA* deletions in populations 4 and 5 was primarily evident in *IDH* mutant tumors (Figures 7A and 7B). Also, *NFKBIA* deletion was associated with shorter patient survival for the subgroups of tumors with either *TERT* mutation or WHO grade 3 class (Figure S4). Median overall survival durations of *TERT* mutant tumors with or without *NFKBIA* deletions were 1.9 vs. 4.3 years in population 4 and 1.4 vs. 3.2 years in population 5, respectively (Figures S4A and S4B). Median overall survival durations of WHO grade 3 gliomas with or without *NFKBIA* deletions were 2.2 vs. 4.6 years in population 4 and 1.7 vs. 14.5 years in population 5, respectively (Figures S4C and S4D).

Since the *NFKBIA* deletion is enriched in recurrent diffuse gliomas (Figure 4A), we examined the association between the deletion and recurrence-free survival. In population 4, *NFKBIA* deletion denoted shorter recurrence-free survival in a two-class model and an adjusted Cox model that included covariates *IDH*, *TERT*, and *ATRX* mutations, 1p19q codeletion, WHO grade, tumor histology, patient age, and patient gender (Figure S5).

Deletions of *NFKBIA* during glioma progression

Of 180 diffuse—WHO grade 2–4—gliomas from population 6, 42 (23.3%) carried *NFKBIA* deletions. Among 87 matched pairs of primary and recurrent tumors, 30 (34.5%) pairs had *NFKBIA* deletions in the primary tumor, the recurrent tumor, or both (Figure 4A). Among the 30 patients with *NFKBIA* deletions, 27 (90%) retained the deletion or acquired a new deletion during tumor progression (Figure 4A). Deletions were more frequent in recurrent tumors (31.0%) than in primary tumors (16.1%) (Figure 4A). Among 74 multiply recurrent tumors, the deletion frequency was even higher
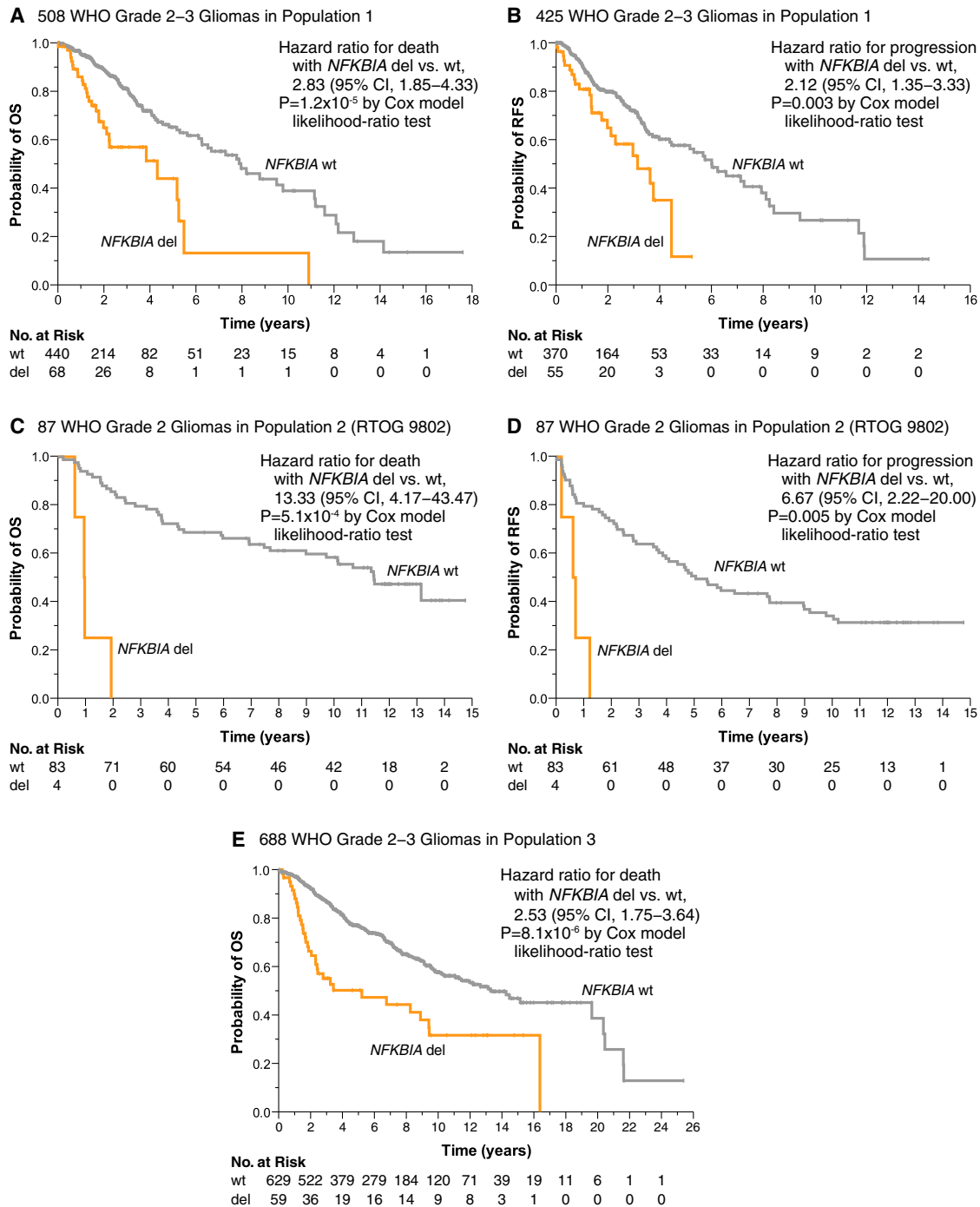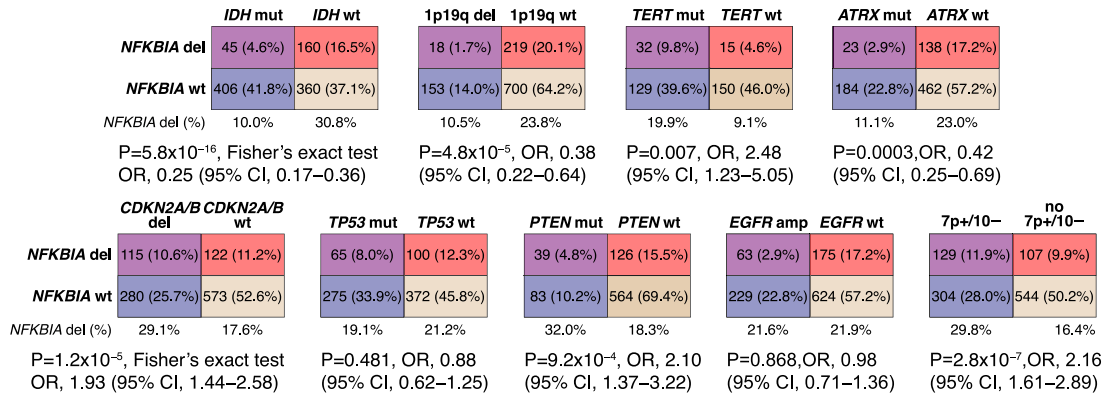
Figure 2. *NFKBIA* deletions and survival in patients with lower-grade gliomas

(A–B) Kaplan-Meier estimates of overall survival (A) and recurrence-free survival (B) for 508 and 425 patients in population 1, respectively, with patients stratified according to the presence (del) or absence (wild-type, wt) of the *NFKBIA* deletion. CI denotes confidence interval. Small vertical lines indicate patients alive at last follow-up assessment. p values were calculated using the Cox model likelihood-ratio test. Patients at risk (No. at Risk) correspond to the x axis timescale.
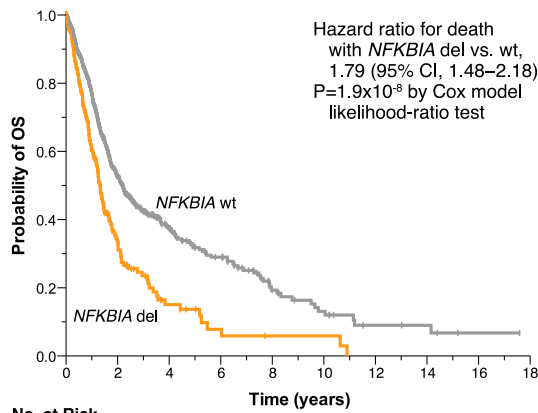
(C and D) Kaplan-Meier estimates for the relationship between *NFKBIA* deletions and patient overall survival (C) and recurrence-free survival (D) in 87 low-grade gliomas patients of NRG/RTOG consortium trial 9802 (population 2).

(E) Kaplan-Meier estimates for the relationship between *NFKBIA* deletions and overall survival in population 3.
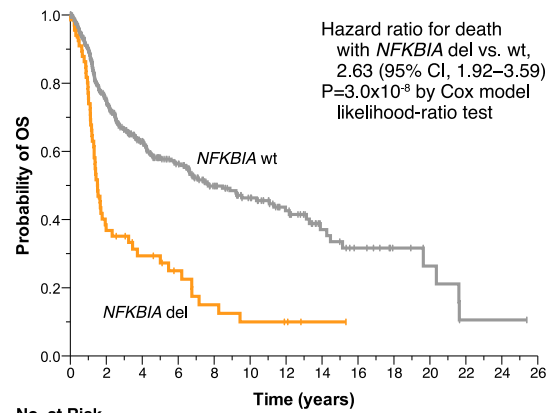
A 1122 WHO Grade 2–4 Gliomas in Population 4

	IDH mut	IDH wt		1p19q del	1p19q wt		TERT mut	TERT wt		ATRX mut	ATRX wt
NFKBIA del	45 (4.6%)	160 (16.5%)		18 (1.7%)	219 (20.1%)		32 (9.8%)	15 (4.6%)		23 (2.9%)	138 (17.2%)
NFKBIA wt	406 (41.8%)	360 (37.1%)		153 (14.0%)	700 (64.2%)		129 (39.6%)	150 (46.0%)		184 (22.8%)	462 (57.2%)
NFKBIA del (%)	10.0%	30.8%		10.5%	23.8%		19.9%	9.1%		11.1%	23.0%

P=5.8x10⁻¹⁶, Fisher's exact test
OR, 0.25 (95% CI, 0.17–0.36)

P=4.8x10⁻⁵, OR, 0.38 (95% CI, 0.22–0.64)

P=0.007, OR, 2.48 (95% CI, 1.23–5.05)

P=0.0003,OR, 0.42 (95% CI, 0.25–0.69)

	CDKN2A/B del	CDKN2A/B wt		TP53 mut	TP53 wt		PTEN mut	PTEN wt		EGFR amp	EGFR wt		7p+/10−	no 7p+/10−
NFKBIA del	115 (10.6%)	122 (11.2%)		65 (8.0%)	100 (12.3%)		39 (4.8%)	126 (15.5%)		63 (2.9%)	175 (17.2%)		129 (11.9%)	107 (9.9%)
NFKBIA wt	280 (25.7%)	573 (52.6%)		275 (33.9%)	372 (45.8%)		83 (10.2%)	564 (69.4%)		229 (22.8%)	624 (57.2%)		304 (28.0%)	544 (50.2%)
NFKBIA del (%)	29.1%	17.6%		19.1%	21.2%		32.0%	18.3%		21.6%	21.9%		29.8%	16.4%

P=1.2x10⁻⁵, Fisher's exact test
OR, 1.93 (95% CI, 1.44–2.58)

P=0.481, OR, 0.88 (95% CI, 0.62–1.25)

P=9.2x10⁻⁴, OR, 2.10 (95% CI, 1.37–3.22)

P=0.868,OR, 0.98 (95% CI, 0.71–1.36)

P=2.8x10⁻⁷,OR, 2.16 (95% CI, 1.61–2.89)

B 1027 WHO Grade 2–4 Gliomas in Population 4

Hazard ratio for death with NFKBIA del vs. wt, 1.79 (95% CI, 1.48–2.18) P=1.9x10⁻⁸ by Cox model likelihood-ratio test

No. at Risk
wt	804	215	88	51	21	12	5	4	1
del	223	39	11	4	2	2	0	0	0

Adjusted Cox Proportional-Hazards Model			
	HR*	95% CI	P-value
NFKBIA del	2.07	1.22–3.53	0.007
IDH mutation	0.16	0.04–0.64	0.010
1p19q codel	1.26	0.22–7.12	0.790
TERT mutation	0.82	0.28–2.39	0.716
ATRX mutation	1.19	0.36–3.86	0.777
WHO Grade			
2 v. 4	0.42	0.17–1.05	0.063
3 v. 4	0.99	0.50–1.93	0.968
Histology			
Oligo v. Astro	0.47	0.20–1.12	0.089
Mixed v. Astro	0.53	0.25–1.12	0.098
Patient age	1.07	1.04–1.09	<0.0001
Patient gender	0.98	0.61–1.60	0.943
CDKN2A/B del	1.24	0.60–2.57	0.562
TP53 mutation	0.92	0.39–2.19	0.851
PTEN mutation	0.55	0.26–1.18	0.125
EGFR amp	0.62	0.31–1.24	0.176
Chr +7/−10	1.23	0.54–2.78	0.630

*hazard ratio for death

C 473 WHO Grade 2–4 Gliomas in Population 5

Hazard ratio for death with NFKBIA del vs. wt, 2.63 (95% CI, 1.92–3.59) P=3.0x10⁻⁸ by Cox model likelihood-ratio test

No. at Risk
wt	407	257	165	120	79	60	40	21	14	8	5	1	1
del	66	22	15	10	6	4	3	1	0	0	0	0	0

Adjusted Cox Proportional-Hazards Model			
	HR*	95% CI	P-value
NFKBIA del	2.23	1.34–3.71	0.002
IDH mutation	0.26	0.07–0.97	0.045
1p19q codel	0.09	0.01–0.75	0.026
TERT mutation	1.34	0.56–3.17	0.511
ATRX mutation	0.82	0.26–2.56	0.730
WHO Grade			
2 v. 4	0.54	0.19–1.50	0.234
3 v. 4	0.71	0.38–1.33	0.287
Histology			
Oligo v. Astro	2.11	0.36–12.23	0.407
Mixed v. Astro	0.98	0.43–2.20	0.951
Patient age	1.03	1.01–1.05	0.004
Patient gender	1.09	0.69–1.70	0.721

*hazard ratio for death

Figure 3. NFKBIA deletions in WHO grade 2–4 gliomas
(A) NFKBIA deletions in relation to driver genetic alterations—the IDH, TERT, ATRX, TP53, and PTEN mutations, 1p19 codeletions, CDKN2A/B deletions, EGFR amplifications, and combined gains of chromosome 7 and monosomy 10 (7+/10−)—in 1,122 WHO grade 2–4 gliomas of population 4. OR, odds ratio; CI, confidence interval.

in the second recurrence (45.5%) (Figures 4A and S6A). These data imply that diffuse gliomas acquire, or select for, *NFKBIA* deletions during disease progression.

Deletion of *NFKBIA* and molecular glioma subtype

Gliomas have seven cohesive methylation subtypes: three *IDH* mutant subtypes (G-CIMP-low, G-CIMP-high, and Codel) and four *IDH* wild-type subtypes (classic-like, mesenchymal-like, LGm6-GBM, and pilocytic astrocytoma-like).[4] In population 4, *NFKBIA* deletions were particularly enriched in three glioma subtypes with low epigenomic DNA methylation[2,29]: *IDH* mutant G-CIMP-low (32.0%), *IDH*-wild-type mesenchymal-like (42.1%), and LGm6 (42.5%) gliomas (Figure 4B). Among *IDH* mutant gliomas, the G-CIMP-low subtype carries a particularly dismal prognosis.[4,16] Despite their cosegregation with this unfavorable subtype (Figure S6B), *NFKBIA* deletions remained independently associated with survival in an adjusted Cox model that included as covariates the methylation subtypes and *IDH, TERT, ATRX, TP53,* and *PTEN* mutations, 1p19q codeletion, *CDKN2A/B* deletion, chromosome 7 gain/10 loss, *EGFR* amplification, WHO grade, tumor histology, and patient age and gender (Figure S6C).

NFKBIA deletion is associated with epigenome hypomethylation

We identified genome-wide methylation targets of the *NFKBIA* deletion in the 609 gliomas of population 4 from genome methylation data. Tumors with *NFKBIA* deletions had a distinct epigenome footprint of widespread DNA hypomethylation (Figure 4C and Table S3); it encompassed 26.3% of all genes with *NFKBIA* regulatory regions (Figure S6D and Table S3)[24] and was highly enriched for pan-glioma CpGs, by whose prevalence gliomas can be classified into distinct DNA methylation subtypes (Figure 4C and Table S3).[4] This was particularly prominent for CpGs whose prevalence robustly distinguishes the two discrete subtypes of 1p19q non-codeleted *IDH* mutant gliomas, the G-CIMP-high vs. G-CIMP-low subtype (Figure 4C and Table S3).[4]

In *IDH* mutant gliomas in population 4, CpGs hypomethylated in *NFKBIA* deleted tumors (Table S3) overlapped significantly with those hypomethylated in all *NFKBIA* deleted gliomas (73.7%) (Figure S6E and Table S3), and the association of those CpGs, whose presence denotes the G-CIMP-low subtype, remained highly significant (Figure S7A).

We validated the epigenomic hypomethylation signature associated with *NFKBIA* deleted gliomas in 87 low-grade gliomas of population 2 for whom whole-genome DNA methylome data were generated. Almost all CpGs (93.0%) were similarly demethylated in tumors with the *NFKBIA* deletion relative to those without the deletion (Figure 4C and Table S3).

Examination of methylome changes of *NFKBIA* deleted gliomas for functionally related sets of genes in population 4 found that genes hypomethylated in the *NFKBIA* deleted tumors relative to wild-type tumors function in nervous system development, in gliomas in general, and *IDH* mutant gliomas in particular (Figure S7B and Table S3). These genes were highly enriched for a gene cluster in the brain with high-CpG-density promoters bearing trimethylated histone 3 marks (Figure S7C and Table S3). Given this enrichment, the link between DNA and histone methylation[30,31] and the importance of chromatin modifications in the regulation of gene transcription,[32,33] we further examined the epigenomic location of hypomethylated CpG sites relative to distinct histone marks. Most of these CpGs mapped to defined histone modification regions, and their locations notably overlapped with that of the repressive histone 3 lysine 27 (H3K27me3) mark in all gliomas (56%) and in *IDH* mutant gliomas (49%) (Figure 4C and Table S3).
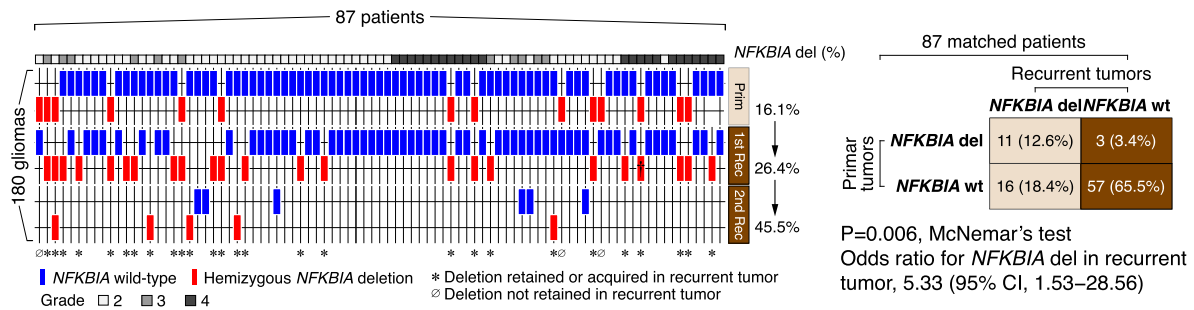
NFKBIA deletion reshapes the DNA and histone methylome antithetically to the *IDH* mutation

Introducing *IDH* mutations into primary human astrocytes establishes the G-CIMP phenotype.[13] The methylation targets of mutant *IDH* in this astrocyte system significantly overlapped with the epigenomic gene signatures of *NFKBIA* deleted and *IDH* mutated/*NFKBIA* deleted gliomas of population 4 (Figure S8A and Table S3). We therefore tested the effects of near-complete small interfering RNA (siRNA)-mediated *NFKBIA* knockdown on epigenome reprogramming in this *IDH1* mutant system. The *NFKBIA* knockdown was associated with reduction in global histone H3K27 trimethylation—a hallmark of promoter activation—in the *IDH1* mutant astrocytes, but less so in parental wild-type astrocytes (Figures 4D and S8B), indicating that the histone hypermethylation landscape engendered by the *IDH* mutation[13,34] is particularly sensitive to *NFKBIA* depletion. Clustered regularly interspaced short palindromic repeats (CRISPR)-mediated *NFKBIA* knockout reduced the global increase in H3K27me3 caused by the *IDH* mutation to an extent similar to that of siRNA-mediated *NFKBIA* knockdown (Figure 4D).
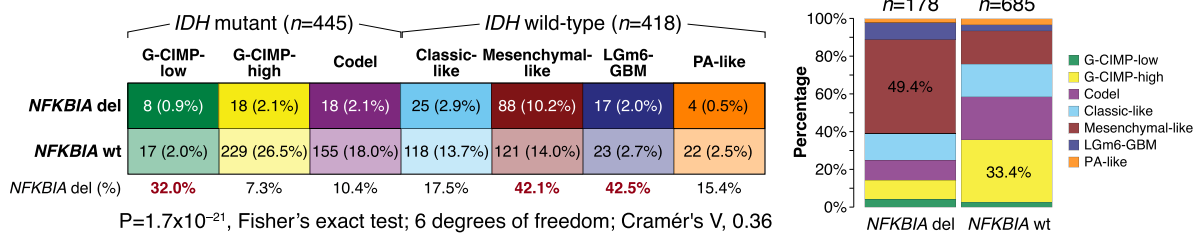
We then assessed the effects of *NFKBIA* knockdown on a representative G-CIMP gene—the monocarboxylate transporter gene *SLC16A3*[13,35]—in the same *IDH1* mutant astrocytes. Although the *SLC16A3* promoter is hypermethylated and enriched for repressive heterochromatin H3K27 and H3K9 marks in these *IDH1* mutant cells,[13] the promoter was hypomethylated in the *NFKBIA* deleted tumors compared with wild-type tumors of population 4 (Figure S8C). NFKBIA can repress gene expression by binding chromatin in regions containing such histone methylation marks.[24] We found that NFKBIA protein directly interacts with the promoter of *SLC16A3* and that *NFKBIA* depletion in these astrocytes reversed the repressive DNA and histone trimethylation marks induced by the *IDH1* mutation, thereby switching the promoter into a transcriptionally active state (Figure 4E). The transcriptional derepression in *NFKBIA*-depleted cells involved reduced binding of NFKBIA to the catalytic PRC2 subunit Enhancer of Zeste 2 (EZH2) (Figure 4E).

(B and C) Kaplan-Meier estimates of overall survival for 1,027 patients in population 4 (B) and 473 patients in population 5 (C), with patients stratified according to the presence (del) or absence (wild-type, wt) of the *NFKBIA* deletion. Small vertical lines indicate patients alive at last follow-up assessment. p values were calculated using the Cox model likelihood-ratio test. Patients at risk (No. at Risk) correspond to the x axis timescale. Bottom panels show corresponding adjusted Cox proportional-hazards models, with *NFKBIA* and other genetic (as available) and clinicopathologic factors as the primary predictor. Hazard ratios for death are displayed for presence vs. absence of the genetic alterations.

**A** 180 WHO Grade 2–4 Gliomas in 87 Patients of Population 6

87 patients

NFKBIA del (%)

180 gliomas

Prim — 16.1%
1st Rec — 26.4%
2nd Rec — 45.5%

∅ ∗ ∗ ∗ ∗   ∗   ∗ ∗ ∗   ∗ ∗ ∗   ∗ ∗   ∗ ∗   ∗   ∗   ∗ ∗ ∗   ∗ ∗∅   ∗∅ ∗   ∗ ∗   ∗

▌ *NFKBIA* wild-type ▌ Hemizygous *NFKBIA* deletion ∗ Deletion retained or acquired in recurrent tumor
Grade ☐ 2 ▨ 3 ■ 4 ∅ Deletion not retained in recurrent tumor

87 matched patients

Recurrent tumors

	NFKBIA del	*NFKBIA* wt
Primary tumors — *NFKBIA* del	11 (12.6%)	3 (3.4%)
NFKBIA wt	16 (18.4%)	57 (65.5%)

P=0.006, McNemar's test
Odds ratio for *NFKBIA* del in recurrent tumor, 5.33 (95% CI, 1.53–28.56)

B 1122 WHO Grade 2–4 Gliomas in Population 4

	IDH mutant (*n*=445)			*IDH* wild-type (*n*=418)			
	G-CIMP-low	G-CIMP-high	Codel	Classic-like	Mesenchymal-like	LGm6-GBM	PA-like
NFKBIA del	8 (0.9%)	18 (2.1%)	18 (2.1%)	25 (2.9%)	88 (10.2%)	17 (2.0%)	4 (0.5%)
NFKBIA wt	17 (2.0%)	229 (26.5%)	155 (18.0%)	118 (13.7%)	121 (14.0%)	23 (2.7%)	22 (2.5%)
NFKBIA del (%)	**32.0%**	7.3%	10.4%	17.5%	**42.1%**	**42.5%**	15.4%

P=1.7x10⁻²¹, Fisher's exact test; 6 degrees of freedom; Cramér's V, 0.36

n=178 *n*=685

49.4%   33.4%

■ G-CIMP-low
■ G-CIMP-high
■ Codel
■ Classic-like
■ Mesenchymal-like
■ LGm6-GBM
■ PA-like

NFKBIA del   *NFKBIA* wt

C 609 WHO Grade 2–4 Gliomas in Population 4 and 87 WHO Grade 2 Gliomas in Population 2 (RTOG 9802)

a 16,041 CpGs (**3.3%**) hypomethylated in *NFKBIA* del vs. wt tumors (FDR-adjusted P<0.001)
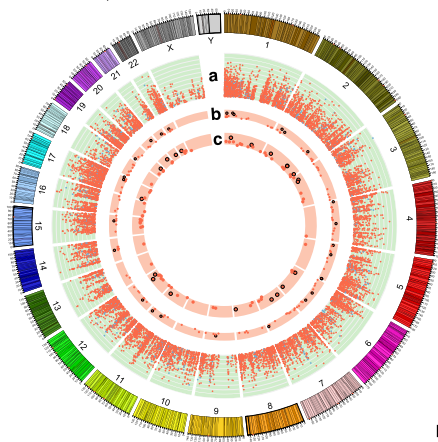
● Validated hypomethylated CpGs in *NFKBIA* del vs. wt (**93.0%**, FDR <0.1)
● Non-validated CpGs

b Overlap with pan-glioma-specific CpGs:

NFKBIA del

	non-hypomethyl CpGs	hypomethyl CpGs	
pan-glioma CpGs	155	1,145	**13.5%**
other CpGs	15,886	468,391	

P=3.2x10⁻⁴², Fisher's exact test
Odds ratio, 3.99 (95% CI, 3.36–4.74)

c Overlap with *IDH* mut (G-CIMP-low/high)-specific CpGs:

NFKBIA del

	non-hypomethyl CpGs	hypomethyl CpGs	
IDH mut/G-CIMP low vs. high specific CpGs	89	42	**67.9%**
other CpGs	15,952	469,536	

P=1.1x10⁻⁹⁸, Fisher's exact test
Odds ratio, 62.37 (95% CI, 43.20–90.04)

Enrichment of hypomethylated CpGs for repressive H3K27me3 marks:

56%   *NFKBIA* del

	non-hypomethyl CpGs	hypomethyl CpGs
CpGs mapping into repressive H3K27me3 marks	8,982	185,248
other CpGs	7,059	284,288
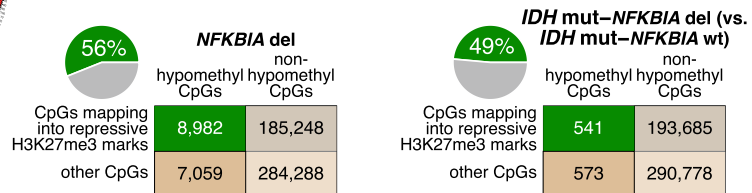
P=0, Fisher's exact test
Odds ratio, 1.95 (95% CI, 1.89–2.02)

49%   *IDH* mut–*NFKBIA* del (vs. *IDH* mut–*NFKBIA* wt)

	non-hypomethyl CpGs	hypomethyl CpGs
CpGs mapping into repressive H3K27me3 marks	541	193,685
other CpGs	573	290,778

P=1.2x10⁻⁹, Fisher's exact test
Odds ratio, 1.44 (95% CI, 1.28–1.62)

D *IDH1-R132H* Mutant Human Astrocytes

si-Ctrl si-*NFKBIA* crispr-Ctrl crispr-*NFKBIA*

NFKBIA
IDH1
β-Actin

global H3K27me3

*P <0.05

☐ si-Ctrl ■ si-*NFKBIA* ☐ cr-Ctrl ■ cr-*NFKBIA*

% Methylation

E *IDH1-R132H* Mutant Human Astrocytes

SLC16A3 G-CIMP gene/promoter   *P <0.05

mRNA   NFKBIA binding   5-mC   H3K27me3   H3K9me3   EZH2

Avg fold (RQ)   % Input
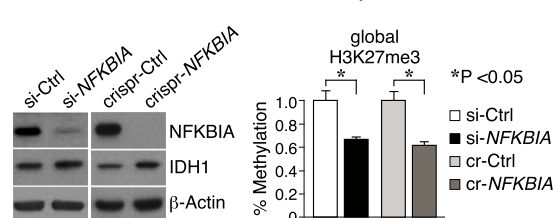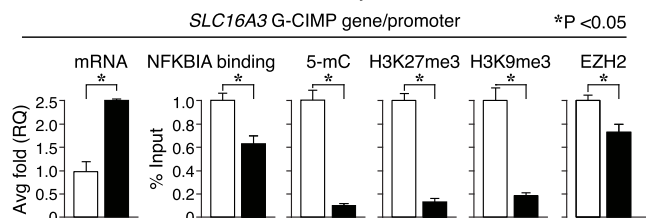
(legend on next page)

To characterize the antipodal epigenome effects of *NFKBIA* deletion and *IDH* mutation, we performed chromatin immunoprecipitation sequencing (ChIP-seq) for H3K27me3 in the primary human astrocyte system with and without *NFKBIA* depletion. This cell system contains a nuclear, chromatin-bound form of phosphorylated-sumoylated (ps-)NFKBIA—which interacts with histones 2A and 4, thereby modulating polycomb recruitment[24]—that is lost upon *NFKBIA* depletion (Figure 5A). Consistent with the effect in the global H3K27me3 assay (Figure S8B), a discrete set of 678 of 13,494 (5.0%) sequenced genes lost H3K27me3 peaks upon *NFKBIA* depletion (Table S4). These genes greatly overlapped with genes CpG hypermethylated upon introducing the *IDH1* mutation (36.6%) and those CpG hypermethylated in the G-CIMP phenotype (36.3%) (Figure 5B and Table S4), suggesting that these genetic events have opposed epigenome effects. Over-representation analysis revealed highly significant enrichment of these genes for functions in development and synaptic plasticity and transmission (Figure 5C).

Much of the H3K27me3-depleted gene set (33.8%) mapped into known H3K27me3 silencer regions (Figure 5D and Table S4). Eighty-five genes (12.5%) mapped to super-silencer regions (Figure 5D and Table S4).[36] These H3K27me3-rich genomic regions (MRRs), defined from clusters of H3K27me3 peaks, silence gene expression via proximity or looping.[36] This gene set included 113 (16.7%) genes responsive to EZH2 inhibition (Figure 5D and Table S4).[36]

PRC2 subcomplexes defined by distinct accessory proteins, PRC2.1 (MTF2) and PRC2.2 (JARID2), synergistically orchestrate H3K27me3 methylation.[37] Their loss primes lineage choice during exit of pluripotency.[38] While MTF2-containing PRC2.1 broadly balances poised lineage-specific gene activation, JARID2-containing PRC2.2 is more selective.[38] In analyzing transcription factor DNA-binding sites for the overlapping set of 85 MRR-associated genes, we found binding sites for the PRC2 core complex (SUZ12 and EZH2) and significant enrichment for binding sites targeted by accessory proteins MTF2 (PRC2.1) and JARID2 (PRC2.2), sug-

gesting that loss of both PRC2 subcomplexes is required for mislocalization of PRC2 and thus loss of H3K27me3 upon *NFKBIA* depletion (Figure 5E and Table S4).[37] Moreover, consistent with data indicating that JARID2-PRC2.2 chromatin association depends on PRC1,[37] we found significant enrichment for polycomb group (PcG) protein BMI1-binding sites, which regulates PRC1 architecture,[39,40] and for PcG protein RNF2-binding sites, the enzymatic component of PRC1 that plays an important role in the migration and differentiation of neural progenitor cells (Figure 5E and Table S4).[40,41]

NFKBIA deletion induces D-2-hydroxyglutarate but not NF-κB in *IDH* mutant cells

The *IDH1* mutation imparts the ability to produce the oncometabolite D-2-hydroxyglutarate (D-2HG).[42] D-2HG levels generated from α-ketoglutarate (α-KG) inhibit demethylases, thus favoring an epigenetic state of high H3K27me3.[43] We measured D-2HG levels in the parental wild-type astrocyte and *IDH1* mutant astrocyte system with and without *NFKBIA* depletion. As expected, D-2HG levels increased more in *IDH1* mutant cells than in wild-type cells without *NFKBIA* depletion (Figure 5F). *NFKBIA* depletion and consequent H3K27me3 loss raised D-2HG production in *IDH1* mutant astrocytes but not in the parental system (Figure 5F). Thus, *NFKBIA* depletion moves the *IDH1* mutant hypermethylated system toward a compensatory loop that inhibits demethylation. *NFKBIA* deletion and *IDH* mutation appear to affect a shared methylation pathway in opposing ways, each with its preferred epigenetic state.

Given *NFKBIA*'s regulation of NF-κB[23] and NF-κB's role in glioma propagation and resistance,[44,45] we analyzed, with DNA-binding ELISAs, the activation state of NF-κB family proteins p65, p50, RelB, and c-Rel in the same astrocyte system with and without *NFKBIA* depletion. We found no biologically meaningful difference in the DNA binding of individual NF-κB proteins upon *NFKBIA* depletion (Figure 5G), indicating that activation of NF-κB is not a primary feature of *NFKBIA* loss in this cell system.

Figure 4. The epigenome landscape of *NFKBIA* deleted gliomas

(A) Deletion (del) frequencies of *NFKBIA* in matched primary tumors vs. first and second recurrence in 180 glioma samples belonging to 87 WHO grade 2–4 gliomas in population 6. †Tumor lost a second *NFKBIA* allele during progression. CI denotes confidence interval.
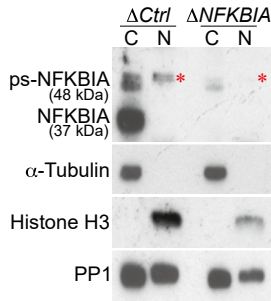
(B) Contingency table of relationships between *NFKBIA* deletions and seven methylation subtypes of glioma in 1,122 WHO grade 2–4 gliomas of population 4. Cramér's V indicates effect size. Panel on the right shows frequencies of these methylation subtypes according to *NFKBIA* status.

(C) Circular genome (CIRCOS) visualization of DNA regions (or CpG sites) hypomethylated in *NFKBIA* deleted vs. wild-type gliomas (false discovery rate [FDR] < 0.001). Data were generated in 609 WHO grade 2–4 gliomas of population 4 and validated in 87 WHO grade 2 gliomas of population 2. Orange dots in ring "a" denote genome-wide CpGs validated with an FDR of <0.1 (93.0%), blue dots denote non-validated CpGs. Orange dots in rings "b" and "c" indicate overlap of these hypomethylated CpGs with CpG signatures found to denote glioma methylation subtypes ("pan-glioma-specific") or to distinguish G-CIMP-low from G-CIMP-high *IDH* mutant tumors. The height of each ring represents the beta-value—the ratio of methylated probe intensity and the sum of methylated and unmethylated probe intensities—difference range of [0.15, 0.3] between *NFKBIA* wild-type and deleted tumors. Dots (CpG sites) with an absolute beta difference of ≥0.2 are encapsulated by a black line. Corresponding two-way contingency tables show cosegregation between CpGs hypomethylated in *NFKBIA* deleted tumors and these CpG signatures. Also shown are two-way contingency tables for the cosegregation of CpGs hypomethylated in *NFKBIA* deleted tumors in general or in the subpopulation of *IDH* mutant tumors with *NFKBIA* deletion and CpGs that map into repressive trimethylated histone 3 lysine 27 (H3K27me3) marks. CI denotes confidence interval.
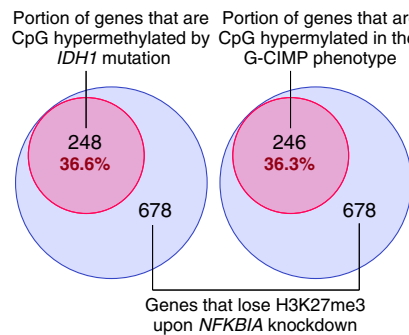
(D) NFKBIA protein expression in primary cultures of human astrocytes carrying the *IDH1-R132H* mutation after siRNA-mediated near-complete (si-*NFKBIA*) knockdown or CRISPR-mediated (crispr [cr]-*NFKBIA*) knockout, compared with scrambled control (Ctrl) versions. β-Actin as a loading control. Panel on the right shows global H3K27me3 levels in si-*NFKBIA* knockdown and crispr-*NFKBIA* knockout cells compared with control cells. Wilcoxon rank-sum test. Error bars represent standard error of the mean (±SEM) from three biological replicates.

(E) Bar graphs show mRNA expression—by real-time PCR average (avg) fold relative quantification (RQ)—of the *SLC16A3* glioma CpG island methylator phenotype (G-CIMP) gene, its promoter binding to NFKBIA or the PRC2 catalytic subunit EZH2, and the promoter's 5-methylcytosine (5-mC) and repressive H3K27me3 and H3K9me3 marks—all based on chromatin immunoprecipitation (ChIP) and expressed as percent of input sample representing the amount of chromatin used in ChIP—following si-*NFKBIA* knockdown in *IDH* mutant primary human astrocytes compared with their control counterparts. Wilcoxon rank-sum test. Error bars represent ±SEM from three biological replicates.
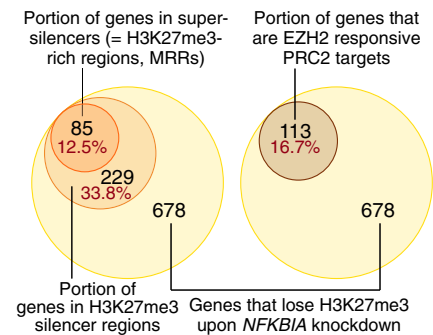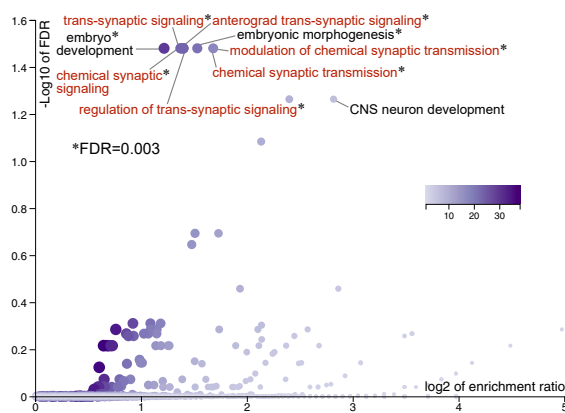
A Immortalized Primary Human Astrocytes

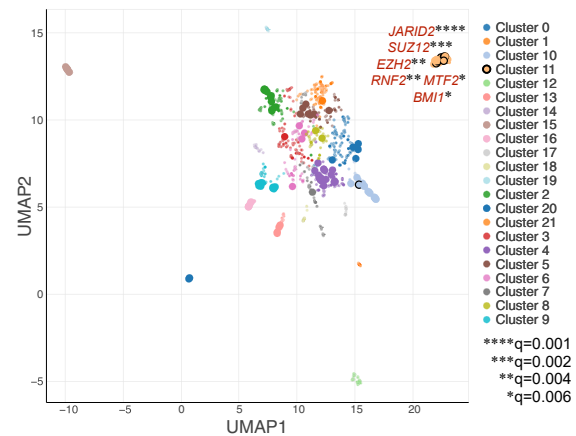**B** Immortalized Primary Human Astrocytes

Portion of genes that are CpG hypermethylated by *IDH1* mutation — 248, **36.6%**, 678

Portion of genes that are CpG hypermylated in the G-CIMP phenotype — 246, **36.3%**, 678

Genes that lose H3K27me3 upon *NFKBIA* knockdown

D Immortalized Primary Human Astrocytes

Portion of genes in super-silencers (= H3K27me3-rich regions, MRRs) — 85, 12.5%; 229, 33.8%; 678

Portion of genes that are EZH2 responsive PRC2 targets — 113, 16.7%; 678

Portion of genes in H3K27me3 silencer regions

Genes that lose H3K27me3 upon *NFKBIA* knockdown

C 248 genes that lose H3K27me3 marks upon *NFKBIA* knockdown and are hypermethylated by *IDH1* mutation

trans-synaptic signaling* / anterograd trans-synaptic signaling*
embryo* / embryonic morphogenesis*
development
modulation of chemical synaptic transmission*
chemical synaptic* signaling / chemical synaptic transmission*
regulation of trans-synaptic signaling* / CNS neuron development

*FDR=0.003

-Log10 of FDR (y-axis) / log2 of enrichment ratio (x-axis)

E 85 genes that lose H3K27me3 marks upon *NFKBIA* knockdown and map into super-silencers (=H327me3-rich regions, MRRs)

*JARID2****
SUZ12***
EZH2** MTF2*
RNF2**
BMI1*

Cluster 0–21

****q=0.001
***q=0.002
**q=0.004
*q=0.006

F *IDH1* wt/mut Human Astrocytes

D-2HG (nmol)

cr-Ctrl / cr-*NFKBIA* (*IDH1* wt)
cr-Ctrl / cr-*NFKBIA* (*IDH1* mut)

*P <0.05
**P=0.001
***P=0.0001

G *IDH1* wt/mut Human Astrocytes

DNA binding

p65 — n.s.
p50 — n.s.
RelB — P<0.05
c-Rel

● *IDH1* wt/Ctrl   ■ *IDH1* wt/si-*NFKBIA*   ▲ *IDH1* wt/cr-*NFKBIA*
▼ *IDH1* mut/Ctrl   ◆ *IDH1* mut/si-*NFKBIA*   ● *IDH1* mut/cr-*NFKBIA*

H

NFKBIA del
NFKBIA wt
K27M
releases / recruits / sequesters
PRC2 EZH2
K27 / K27me3
Active chromatin/demethylated DNA
Histone H3
Silent chromatin/methylated DNA
Demethylases
5-mC
D-2HG
α-KG
mIDH

NFKBIA del
H3K27M
NFKBIA del/*mIDH* / *mIDH*

I 702 WHO Grade 2–4 Gliomas in Population 4 and Human Embryonic Stem Cells

P=2.0x10⁻¹⁸
OR, 2.60 (2.15–3.15)

H3K27me3 targets in hES — 405
61
62
590 — PRC2 targets in hES
2506 — Genes up in *NFKBIA* del

P=1.7x10⁻⁷
OR, 2.17 (1.66–2.83)
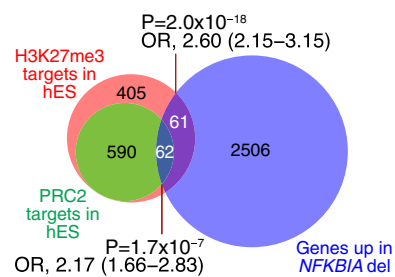
(legend on next page)

NFKBIA deletion induces a transcriptome landscape reminiscent of that of *H3K27M* mutant gliomas

Unmethylated CpG islands are high-affinity sites for PRC2.[46,47] PRC2 modifies chromatin structure as its catalytic EZH2 subunit deposits H3K27me3 (Figure 5H).[48] Chromatin-bound NFKBIA regulates differentiation-related genes by recruiting PRC2 (Figure 5H), and genomic sequences occupied by NFKBIA strongly overlap with those having high levels of H3K27me3.[24] Genes hypermethylated in *IDH* mutant gliomas are greatly enriched for PRC2-targeted loci,[13] and the mutation increases global H3K27me3 levels by competitively inhibiting demethylases (Figure 5H).[49] *H3K27M* mutant diffuse midline gliomas demonstrate defective H3K27me3 deposition due to PRC2 sequestration, especially from large unmethylated CpG islands (Figure 5H).[46,50,51] Given our observed enrichment for demethylated CpGs mapping to genes bearing repressive H3K27me3 marks in *NFKBIA* deleted gliomas, we examined whether the transcriptome landscape in these tumors shares features associated with the *H3K27M* mutation in diffuse midline gliomas.[17,46,52–54]

We analyzed 2,629 genes significantly overexpressed in *NFKBIA* deleted vs. *NFKBIA* wild-type gliomas (*NFKBIA* deletion signature) in population 4 (Table S4) by comparing them with the presence of H3K27me3 or PRC2 target genes in undifferentiated human embryonic stem cells.[55] We found a highly significant intersection of the *NFKBIA* deletion signature with both H3K27me3- and PRC2-target genes (Figure 5I and Table S4). The *NFKBIA* deletion signature overlapped significantly with the presence of genes upregulated in *H3K27M* mutant DIPGs compared with *H3K27* wild-type DIPGs in population 7 (comprising 11 patients with *H3K27M* mutations and 5 with wild-type *H3K27*), in four additional independent datasets of *H3K27M* mutant diffuse midline gliomas, and in an inducible *H3K27M* DIPG model (Figures 6A, 6B, and S9A; Table S4).

H3K27me3 marks undergo genomic redistribution in the *H3K27M* mutant condition.[46,52,56] Strikingly, the *NFKBIA* deletion signature closely resembled the pattern of H3K27 receptive genes specific to *H3K27M* but less so those specific to *H3K27WT* tumors (Figure 6A and Table S4). Functional enrichment analysis of gene signature interaction between *NFKBIA* deleted gliomas and *H3K27M* mutant diffuse midline gliomas revealed—similar to that between *NFKBIA* deletion and *IDH1* mutation (Figure 5B)—significant over-representation of functions in neurogenesis and synaptic plasticity (Figure 6B and Table S4). To exclude the possibility that the enriched overlap of genes reflected *IDH* mutation status, we assessed the intersection and functional enrichment in *IDH* mutant tumors. We again noted significant intersection between genes hypomethylated in *IDH* mutant/*NFKBIA* deleted (vs. *IDH* mutant/*NFKBIA* wild-type) gliomas and genes derepressed in *H3K27M* mutant diffuse midline gliomas (Figure S9B and Table S5). These overlapping genes demonstrated significant over-representation of functions in neurogenesis and synaptic plasticity, such as regulation of trans-synaptic signaling and modulation of chemical synaptic transmission (Figure S9B).

To examine the biological similarity of the molecular consequences of *H3K27M* mutation and *NFKBIA* deletion, we tested


Figure 5. *NFKBIA* deletion reshapes the methylome antithetically to the *IDH* mutation

(A) Immunoblot showing expression of NFKBIA in nuclear (N) and cytoplasmic (C) fractions of control (ΔCtrl) and *NFKBIA*-depleted (Δ*NFKBIA*) immortalized primary human astrocytes. Presence of the canonical 37 kDa band in the C fraction captured with anti-phospho-NFKBIA and the ∼48 kDa band in the N fraction of ΔCtrl cells but not Δ*NFKBIA* cells; the latter is compatible with chromatin-bound, phosporylated-sumoylated NFKBIA (ps-NFKBIA) (red asterisks). α-Tubulin as a cytoplasmic and histone H3 as a nuclear loading control. Protein phosphatase 1 (PP1) as a loading control for both soluble and chromatin fractions.

(B) Euler diagrams showing the proportion of 678 genes with loss of repressive H3K27me3 marks by ChIP-seq upon *NFKBIA* depletion in primary cultures of human astrocytes and intersection with genes CpG hypermethylated upon introducing the *IDH1* mutation into the same astrocyte system or with genes CpG hypermethylated in the G-CIMP phenotype.

(C) Functional enrichment analysis of the 248 genes in (A) that lose H3K27me3 marks upon *NFKBIA* depletion and are hypermethylated by the *IDH1* mutation.

(D) Euler diagrams showing the proportions of the same 678 genes that map into H3K27me3 silencer regions or super-silencers (H3K27me3-rich regions, MRRs), and those that are EZH2-responsive PRC2 targets.

(E) Transcription factor binding site analysis for the 85 MRR-associated genes in (D) that overlap with the H3K27me3-depleted gene set. Scatterplot of terms in the ChIP enrichment analysis (ChEA) gene set library. Terms are plotted based on the first two uniform manifold approximation and projection (UMAP) dimensions. Terms with more similar gene sets are closer together. Terms are colored by automatically identified clusters computed with the Leiden algorithm applied to the term frequency-inverse document frequency (TF-IDF) values. Darker and larger points signify more substantial enrichment. Significant enrichment (points encapsulated by a black line) for components of the PRC2 core complex (*SUZ12* and *EZH2*) and accessory proteins that define PRC2 subcomplexes PRC2.1 (*MTF2*) and PRC2.2 (*JARID2*), and other polycomb group (PcG) genes (*BMI1* and *RNF2*). q values calculated by the Benjamini-Hochberg method.

(F) Levels of D-2-hydroxyglutarate (D-2HG) assessed by colorimetric enzymatic assay in primary cultures of *IDH* wild-type (wt) or *IDH1-R132H* mutant (mut) human astrocytes with CRISPR-mediated (cr-*NFKBIA*) or without (cr-Ctrl) *NFKBIA* depletion. Student's t test. Error bars represent ±SEM from three biological replicates.

(G) DNA-binding activity of NF-κB proteins p65, p50, RelB, and c-Rel assessed by DNA-binding ELISAs in *IDH* wt vs. *IDH1-R132H* mut primary human astrocytes transfected with siRNA (si)-*NFKBIA* or cr-*NFKBIA* vs. Ctrl. Multiple-comparison one-way ANOVA with post hoc Tukey's test. Error bars represent ±SEM from three biological replicates. n.s., non-significant.

(H) Graphical model of the relationship between the *NFKBIA* deletion and *IDH* and *H3K27M* mutations and polycomb repressive complex 2 (PRC2). Chromatin-bound NFKBIA ("*NFKBIA* wt") regulates differentiation-related genes by recruiting PRC2, which promotes the trimethylation of H3K27 (H3K27me3) through its catalytic subunit EZH2, a histone methyltransferase. Deletion of *NFKBIA* (*NFKBIA* del) results in PRC2 release and, thus, loss of H3K27me3. Similarly, *H3K27M* mutations in diffuse midline gliomas sequester PRC2, thereby reducing global H3K27me3 levels, especially in large unmethylated CpG islands. In turn, the *IDH* mutation (m*IDH*) hypermethylates DNA (5-mC, 5-methylcytosine) and increases global H3K27me3 levels—particularly at PRC2-targeted loci—by metabolizing α-ketoglutarate (α-KG) to D-2-hydroxyglutarate (D-2HG) and competitively inhibiting DNA and histone demethylases. Tumors with both the *NFKBIA* deletion and the *IDH* mutation demonstrate methylome changes that are more similar to those with an isolated *NFKBIA* deletion than to those with an isolated *IDH* mutation.

(I) Area-proportional Euler diagrams depicting the intersection of genes overexpressed in *NFKBIA* deleted gliomas (*NFKBIA* deletion signature) in population 4 and those identified as H3K27me3 or PRC2 targets in human embryonic stem (hES) cells. OR, odds ratio.
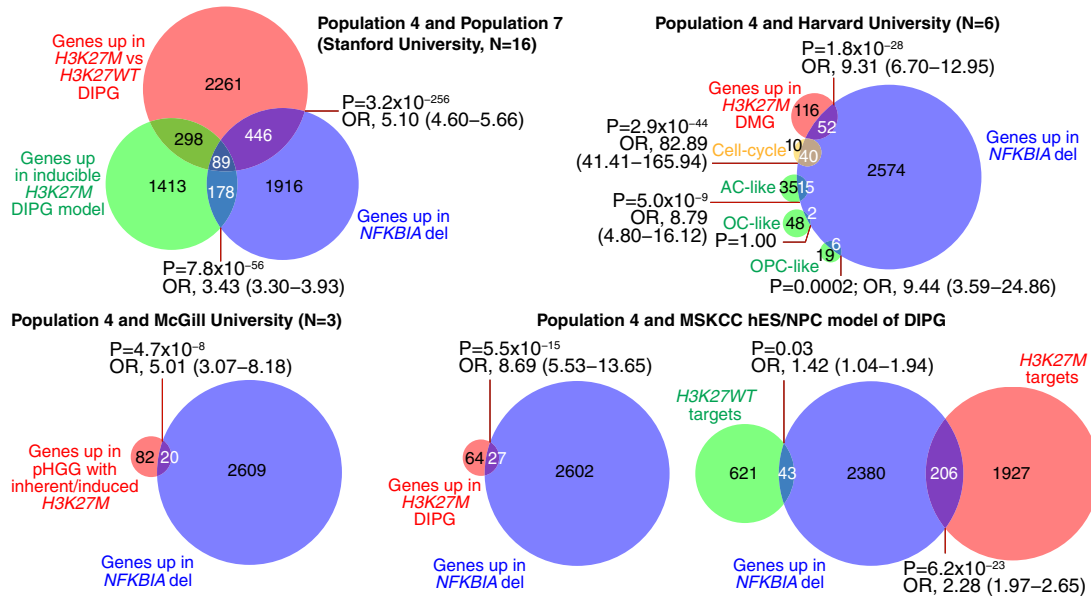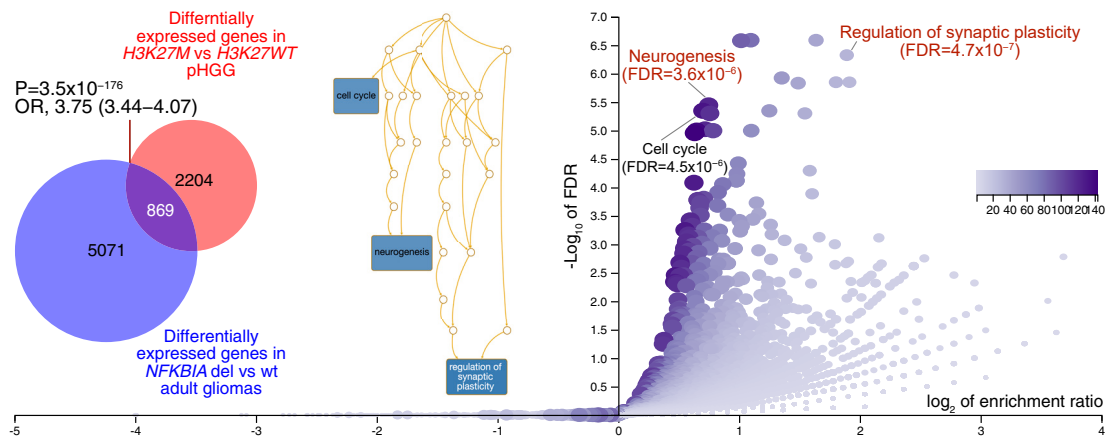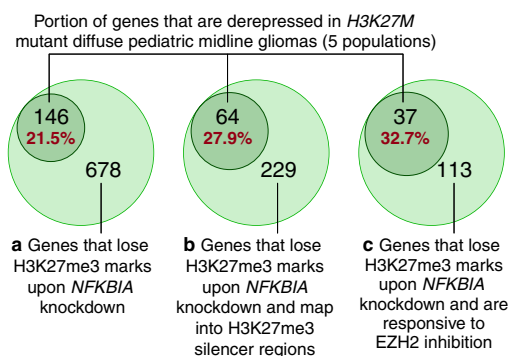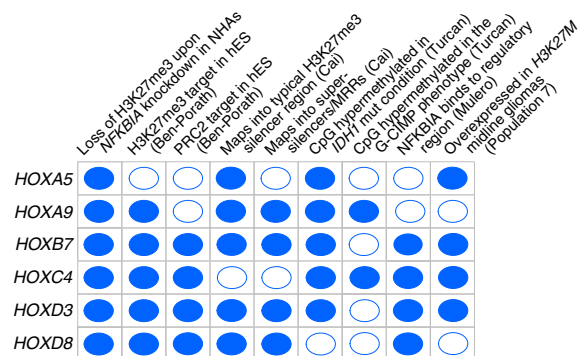
Figure 6. *NFKBIA* deletion gene signature intersects with a gene signature of *H3K27M* mutant diffuse midline glioma

(A) Left upper panel shows an area-proportional Euler diagram depicting the intersection of genes overexpressed in *NFKBIA* deleted gliomas (*NFKBIA* deletion signature) and those overexpressed in a panel of 11 diffuse intrinsic pontine glioma (DIPG) tumor samples from population 7 carrying *H3K27M* mutations compared with five DIPGs that are wild-type for *H3K27* (*H3K27WT*). Intersection between *NFKBIA* deletion signature and genes overexpressed in an inducible pontine model of *H3K27M* mutant DIPG is also shown. Right upper and lower panels show area-proportional Euler diagrams depicting intersection of the *NFKBIA*

(legend continued on next page)

the intersection of genes that lose repressive H3K27me3 upon *NFKBIA* knockdown in the immortalized astrocyte system with genes derepressed in *H3K27M* mutant pediatric midline gliomas: 21.5% of H3K27me3-depleted genes overlapped with genes overexpressed in the *H3K27M* mutant condition and 27.9% of H3K27me3-depleted genes mapped into genomic regions that can silence gene expression via chromatin interactions (Figure 6C and Table S5).[36] Strikingly, about one-third (32.7%) of H3K27me3-depleted genes that are EZH2 responsive PRC2 target genes intersected with genes derepressed in *H3K27M* mutant tumors (Figure 6C and Table S5).

This enriched gene set included a cluster of *HOX* genes (Figure 6D). *HOX* genes are paradigmatic polycomb targets,[57,58] and ps-NFKBIA interacts with histones 2A and 4 at their regulatory region.[24] Several of these *HOX* genes were overexpressed in the *H3K27M* mutant tumors of population 7, possess NFKBIA regulatory regions, constitute H3K27me3 and PRC2 targets in human embryonic stem cells, map into typical H3K27me3 silencer or super-silencer regions (MRRs), and are CpG hypermethylated in the *IDH* mutant condition and the G-CIMP phenotype (Figure 6D). These data indicate that both *NFKBIA* deletion and *H3K27M* mutation can seize a common trimethylation pathway that leads to a de facto PRC2 loss-of-function epigenetic state.

NFKBIA deletion and outcome in *IDH* mutant diffuse gliomas

Although generally more favorable, outcomes of patients with *IDH* mutant gliomas can vary substantially and are difficult to predict. The WHO classification highlights the importance of *CDKN2A/B* deletions and *TP53* mutations in *IDH* mutant gliomas.[12] We found no pattern of occurrence between *NFKBIA* deletions and either of these two alterations (Figure S10A). A two-class model of the relationship between *NFKBIA* and survival duration in patients of population 4 with *IDH* mutant tumors revealed remarkably briefer survival of patients with *NFKBIA* deleted tumors compared with non-deleted tumors, with median survival estimates of 3.8 and 7.6 years, respectively (Figure 7A). This survival association held in an adjusted Cox model that included *IDH*, *ATRX*, *TERT*, and *TP53* mutations, 1p19 codeletions, *CDKN2A/B* deletions, WHO grade, histology, patient

age, and patient gender (Figure S10B). A similar association was found in *IDH* mutant gliomas of population 5: median survival of 6.8 vs. 14.3 years in the *NFKBIA* deleted vs. *NFKBIA* wild-type tumors (Figure 7B); this relationship held in an adjusted Cox model (Figure S10C).

NFKBIA deletion and a nomogram predicting individual patient survival in *IDH* mutant gliomas

Nomograms are graphical representations of statistical models that allow individualized predictions based on the characteristics of a single patient.[59] We generated a nomogram model that uses *NFKBIA* deletion and the best-established clinicopathologic and molecular genetic markers to estimate the probability of 5-year survival of individual patients with *IDH* mutant glioma. In choosing this method, we balanced model sparsity (minimal number of needed variables), interpretability, and predictive accuracy. We used the 398 *IDH* mutant gliomas of population 4 to build, internally validate, and calibrate the model and assess performance over 15 years. This model retained the *NFKBIA* deletion but not the 1p19q codeletion as a significant variable (Figure 7C). We then used the 291 *IDH* mutant gliomas of population 5 to validate the model externally. *NFKBIA* deletion remained an independent survival variable with an effect on survival greater than that of all other variables, including 1p19q codeletion, *TERT* mutation, *ATRX* mutation, WHO grade, and patient age (Figure 7D). Similar models incorporating *CDKN2A/B* deletions and *TP53* mutations in the *IDH* mutant gliomas of population 4 (Figure S11A) or using the 619 *IDH* mutant lower-grade gliomas of populations 1 and 5 (Figure S11B) confirmed that the *NFKBIA* deletion is a robust variable in predicting the duration of survival of patients with *IDH* mutant gliomas.

DISCUSSION

Here, we report chromatin-bound *NFKBIA* to be a haploinsufficient tumor suppressor whose deletion portends an unfavorable clinical course of diffuse gliomas. The patterned presence of the *NFKBIA* deletion with the driver mutations *IDH*, *TERT*, *ATRX*, and *PTEN*, the 1p19q codeletion, the *CDKN2A/B* deletion, and its enriched occurrence in recurrent tumors support the notion that this deletion is a critical genetic event during glioma progression.

---

deletion signature and genes overexpressed in three additional independent validation populations or models of pediatric midline glioma (pHGG, pediatric high-grade glioma; DMG, diffuse midline glioma; DIPG, diffuse intrinsic pontine glioma) carrying *H3K27M* mutations from Harvard University, McGill University, and Memorial Sloan Kettering Cancer Center (MSKCC). Cosegregation of the *NFKBIA* deletion signature with genes delineating cell subpopulations resembling various differentiation states, cell lineages (AC-like, astrocytic differentiation; OC-like, oligodendrocytic differentiation; OPC-like, oligodendrocyte precursor cells-like) and oncogenic programs (cell cycle) are shown for the Harvard population. In the human embryonic stem (hES)/neural progenitor cell (NPC) DIPG model from MSKCC, the *NFKBIA* deletion signature more closely resembled H3K27me3 target genes specific to mutant *H3K27M* than those of wild-type *H3K27*.

(B) Area-proportional Euler diagram depicting the intersection of the *NFKBIA* deletion signature with an *H3K27M* gene expression signature in 119 pediatric high-grade gliomas from Gustave Roussy Paris. Functional enrichment analysis of the intersecting signature of 869 genes between *NFKBIA* deleted gliomas and *H3K27M* diffuse midline gliomas. The relationship between the significant gene ontology functions is visualized in a directed acyclic graph. FDR, false discovery rate. p values from Fisher's exact test.

(C) Euler diagram showing intersection of genes derepressed in *H3K27M* mutant diffuse pediatric midline gliomas (above five populations) and those that lose repressive H3K27me3 marks by ChIP-seq upon *NFKBIA* depletion in primary cultures of human astrocytes (a), those that lose repressive H3K27me3 marks upon *NFKBIA* depletion and map into known silencer regions (b), and those that lose repressive H3K27me3 marks upon *NFKBIA* depletion and are EZH2-responsive PRC2 targets (c).

(D) Intersection of a cluster of *HOX* genes—paradigmatic PRC2 targets—that lose H3K27me3 marks upon *NFKBIA* depletion in primary cultures of human astrocytes with genes overexpressed in the *H3K27M* mutant DIPGs of population 7, those with NFKBIA regulatory regions, those described as H3K27me3 and PRC2 targets in human embryonic stem cells, those that map into typical H3K27me3 silencer and super-silencer regions (MRRs), and those CpG hypermethylated in the *IDH1* mutant condition and the G-CIMP phenotype.
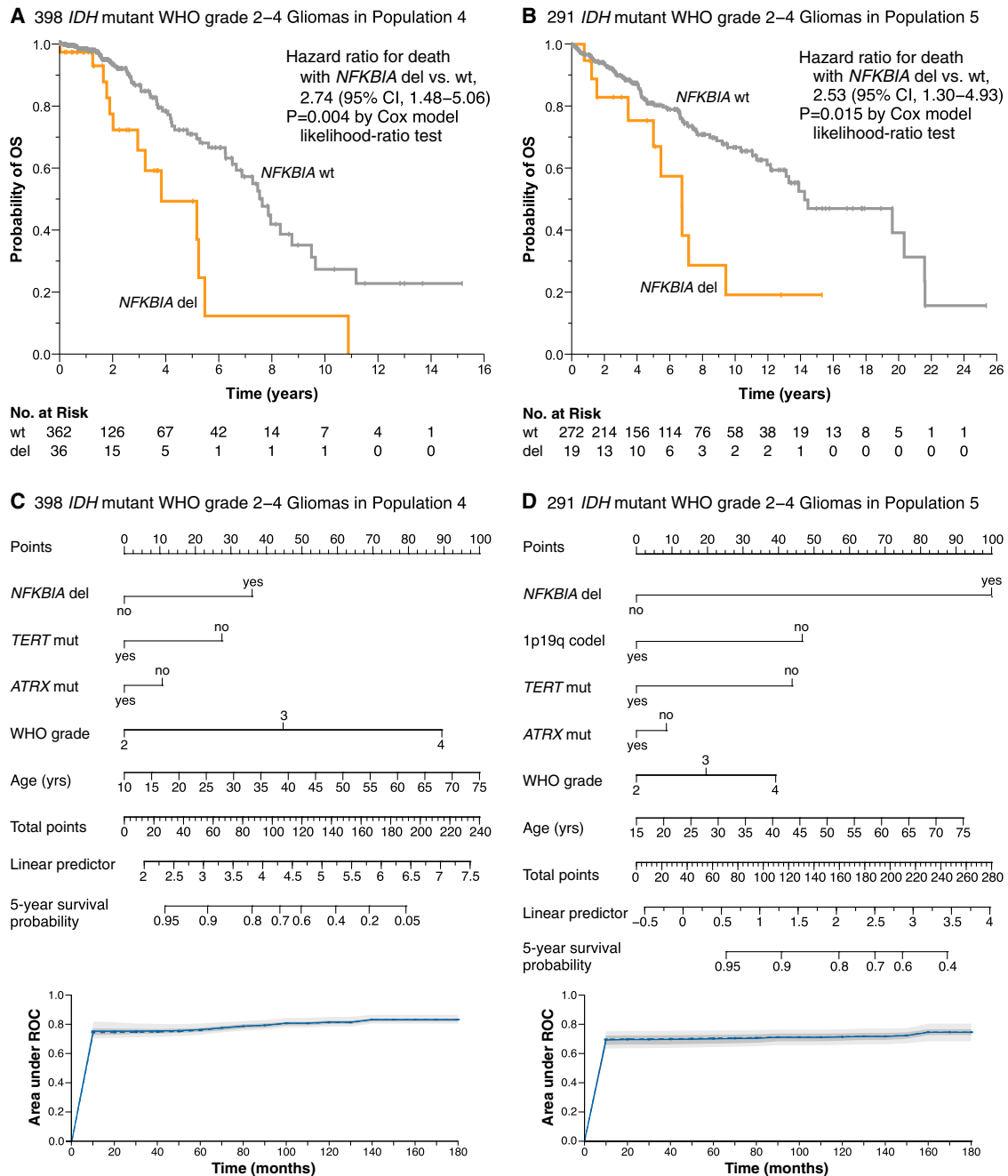
Figure 7. *NFKBIA* deletions and survival in *IDH* mutant WHO grade 2–4 gliomas

(A and B) Kaplan-Meier estimates of overall survival for 398 *IDH* mutant glioma patients in population 4 (A) and 291 *IDH* mutant glioma patients in population 5 (B), with patients stratified according to the presence (del) or absence (wild-type, wt) of the *NFKBIA* deletion. Small vertical lines indicate patients alive at last follow-up assessment. p values were calculated using the Cox model likelihood-ratio test. Patients at risk (No. at Risk) correspond to the x axis timescale.

(C and D) Corresponding nomograms for predicting the probability of survival at 5 years in *IDH* mutant gliomas. Nomograms built based on high-dimensional penalized Cox models using the adaptive least absolute shrinkage and selection operator (adaLASSO) function. Models include the covariates *NFKBIA* deletion, 1p19q codeletion, *TERT*, and *ATRX* mutations, WHO grade, and patient age and were internally validated and calibrated by repeated cross-validation in population 4, then externally validated and calibrated in population 5. Displayed variables are those retained as significant. Model performance by time-dependent area under the receiver-operating curve (ROC) (t-AUC) over 180 months (15 years). Curves reflect average performance for each cross-validation event. The solid line represents the mean of the area under the t-AUC and the dashed line the median of the AUC. The darker interval shows 25% and 75% quantiles of the t-AUC, and the lighter interval shows the minimum and maximum of the t-AUC.

Glioma progression is associated with specific demethylation shifts,[16,60] some of which we found resemble methylome changes related to the *NFKBIA* deletion.

NFKBIA is a critical regulator of NF-κB,[23] which is involved in glioma propagation and resistance.[44,45] Nuclear NFKBIA participates in chromatin-associated epigenetic regulation.[24,25] It does so by dynamically associating with histones H2A and H4 to control a subset of polycomb-regulated differentiation genes, thus governing stem cell maturation and lineage specification.[24,25] Our observations show that *NFKBIA* deletions manifest epigenetically in gliomas in two ways: demethylation of glioma-associated CpG sites and loss of repressive histone H3K27 trimethylation marks. Both effects appear to be antithetical to the DNA and histone methylome changes caused by the *IDH* mutation. Consistently, we found that *IDH* mutant tumors with the *NFKBIA* deletion behave similarly to *IDH* wild-type tumors.

Mutant *IDH* reshapes the epigenome through extensive DNA hypermethylation and increasing repressive histone methylation.[13,49,61] The opposed effects of *NFKBIA* deletion and *IDH* mutation on the glioma epigenome may reflect overlapping but antipodal regulatory roles in chromatin remodeling.[24,62] DNA methylation and histone modifications participate in chromatin organization.[13,30,31] Genes undergoing hypermethylation in response to the *IDH* mutation are highly enriched for PRC2-targeted loci,[13] as DNA methylation and the PRC2 system are intimately linked.[63] Similarly, histone-bound NFKBIA interacts with PRC2 and regulates its association with a subset of target genes.[24,25,64] As such, *NFKBIA* deletion and *IDH* mutation may drive a PRC2-regulated methylome mechanism toward diametrically different epigenetic states.

We also noted that the epigenetic state facilitated through *NFKBIA* deletion partially mimics the altered chromatin landscape of diffuse midline gliomas carrying *H3K27M* oncohistone mutations. *H3K27M* mutations lead to defective spread and significantly lower overall amounts of trimethylated H3K27 by sequestering PRC2 to poised enhancers, wherein PRC2 becomes trapped at *H3K27M*-H3K27me3 boundaries[46,51,52,56]; this engenders discrete transcriptome changes that preferentially involve derepression of genes regulating neurogenesis.[46,54] We found that the methylome changes of *NFKBIA* deleted gliomas are highly enriched for neural stem cell and neurogenesis genes bearing repressive H3K27 marks.[24,30] Moreover, we observed significant overlap between the transcriptomic landscapes of *NFKBIA* deleted and *H3K27M* mutant gliomas, with an over-representation of functions of stemness, neurogenesis, and regulation of synaptic plasticity. This mutual functional enrichment is consistent with compelling evidence indicating that gliomas can manipulate normal elements of neuronal development and synaptic plasticity,[65–67] a process that may be partly driven through PRC2: neuronal activity can derepress PRC2,[68] and PRC2 is a key regulator of epigenetic plasticity in glioblastoma.[69] Consistently, our findings imply that the *NFKBIA* deletion in adult gliomas and the *H3K27M* mutation in pediatric diffuse midline gliomas define aggressive disease subtypes that may share an epigenetic state reflecting a common PRC2 loss-of-function phenotype antipodal to the quasi PRC2 gain-of-function phenotype of *IDH* mutant gliomas and their favorable clinical course. This PRC2 loss-of-function phenotype might become a functionally defined therapeutic target in gliomas as histone demethylase inhibitors successfully enter clinical trials.[70–73]

NFKBIA maps to chromosome 14q13.2. *NFKBIA* may be one of multiple yet-to-be-identified targets that drive 14q losses in gliomas via cumulative haploinsufficiency.[74] While our results contribute to bridging several important gaps in our understanding of how *NFKBIA* haploinsufficiency impacts the biology and clinical behavior of gliomas, wider-spanning losses on the long arm of chromosome 14 have been identified in gliomas.[75–77] These genomic loci map more distally on 14q within commonly deleted regions spanning 14q21.2–14q24.3, 14q22.3–q32.1, 14q31.3–q32.1, and 14q32.1–14qter.[75–77] No other glioma-associated tumor-suppressor genes have been identified within the region encompassing our *NFKBIA* deletion and these more distal regions. Chromosome 14q losses correlate with increased complexity of chromosome copy number. We consistently noted greater copy-number complexity in *NFKBIA* deleted tumors than in non-deleted tumors across every WHO grade of glioma but found that the survival association of *NFKBIA* remained independent of aneuploidy.

Our data show that lower-grade gliomas harboring *NFKBIA* deletions behave much like high-grade gliomas. *NFKBIA* deletions result in a clinical course for *IDH* mutant gliomas that resembles that of *IDH* wild-type tumors. Despite the comparatively favorable prognosis of most *IDH* mutant gliomas, individual outcomes vary greatly. *NFKBIA* status may be a robust marker in identifying *IDH* mutant tumors with potential for more aggressive behavior and thus the need for earlier, more substantial therapy. Accordingly, we generated a clinically applicable and externally validated nomogram model, including *NFKBIA*, to predict the survival duration of patients with *IDH* mutant gliomas. Estimation of survival duration of an individual patient from such a nomogram is highly preferable to estimation based on membership in a subpopulation defined by multiple disease characteristics.[59] Risk grouping forces patients into distinct classes, ignores the individuality of each glioma case, and becomes impractical as more driver genetic events are identified. We developed a linear model that balances the number of selected variables and predictive performance by focusing on *NFKBIA* deletion and current best-established genetic and clinicopathologic factors. It reflects a reasonable compromise between model sparsity—and thus ease of clinical use and interpretability—and accuracy of outcome prediction. While our model consistently and independently associates the *NFKBIA* deletion with survival in multiple well-characterized glioma populations, further validation—ideally in a prospective trial—is needed to ascertain its role in clinical prognostication.

Limitations of the study

Despite the inclusion of seven well-characterized glioma populations, including a national randomized consortium trial, the retrospective nature of our analysis of *NFKBIA* deletions and their correlation with patient outcomes highlights the need for a prospectively conducted cohort study to further affirm the survival significance of *NFKBIA*. To address the issue of model complexity and predictive ability, we developed a linear

nomogram model that focused on the *NFKBIA* deletion, along with the most well-established genetic and clinicopathologic factors, achieving a good balance between the number of selected variables and predictive performance. However, there is a trade-off between model sparsity and precision of outcome predictions, and any future optimizations of this nomogram model will have to consider a balance between model simplicity, interpretability, and predictive accuracy. We used different molecular platforms to characterize *NFKBIA* deletions. A simple yet robust assay to screen for *NFKBIA* deletions would enable wide clinical applicability. Our findings suggest that *NFKBIA* deletions hold significant promise as a biological and clinical target in diffuse gliomas. However, currently, there is no molecular therapeutic intervention that would allow for the specific restitution of *NFKBIA* expression, except for first-generation and second-generation proteasome inhibitors—clinically used in multiple myeloma, mantle cell lymphoma, and some types of non-Hodgkin's lymphoma—that suffer from broad off-target effects. Further research is needed to develop effective and targeted molecular therapies for *NFKBIA* deletions in gliomas.

STAR★METHODS

Detailed methods are provided in the online version of this paper and include the following:

- KEY RESOURCES TABLE
- RESOURCE AVAILABILITY
  - Lead contact
  - Materials availability
  - Data and code availability
- EXPERIMENTAL MODEL AND SUBJECT DETAILS
  - Tumor samples and patient populations
  - Cell lines
- METHOD DETAILS
  - Mutational analyses
  - Copy number analyses
  - Methylome analyses
  - RNA sequencing analyses
  - Fluorescence *in situ* hybridization (FISH)
  - Immunofluorescence
  - Knockdown and knockout of *NFKBIA*
  - mRNA extraction and quantitative polymerase chain reaction (PCR)
  - Protein extraction and immunoblotting
  - Genomic DNA preparation
  - Global histone methylation analysis
  - Chromatin immunoprecipitation (ChIP)
  - ChIP sequencing
  - Transcription factor DNA-binding site analysis
  - D-2-hydroxyglutarate assay
  - NF-κB family protein activation assay
- QUANTIFICATION AND STATISTICAL ANALYSIS

SUPPLEMENTAL INFORMATION

Supplemental information can be found online at https://doi.org/10.1016/j.xcrm.2023.101082.

AUTHOR CONTRIBUTIONS

Conceptualization, M.B.; methodology, M.B., L.E., H.K., D.M.S., J.P.M., and S.L.P.; validation, M.B., D.M.S., and J.P.M.; formal analysis, M.B., L.E., H.K., D.M.S., J.P.M., W.M., T.M.K., T.M.M., M.A.Q., A.W., R.G.W., B.H., J.S.B.-S., H.N., and R.B.J.; investigation, M.B., L.E., H.K., R.R., W.M., T.M.K., T.M.M., M.A.Q., T.L.-J., A.M., L.S., S. Nagaraja, S. Nair, J.J.W., G.R.H., N.K.T., J.L.F., A.N., S.O., J.B., S.J.H., A.-L.G., M.W., J.S.B.-S., M.M., H.N., R.B.J., and A.C.; resources, T.A.C., C.L.R., and D.R.M.; data curation, M.B., H.K., J.P.M., A.W., and S.L.P.; writing – original draft, M.B.; writing – review & editing, all authors; visualization, M.B., H.K., and J.P.M.; supervision, M.B.; project administration, M.B., S.L.P., and A.C.; funding acquisition: M.B., L.E., T.L.-J., M.W., and A.C. All authors discussed the results and commented on the manuscript.

DECLARATION OF INTERESTS

M.B.: NIH/NINDS grant R01NS117641, advisory board membership and grant (Varian Medical Systems), consulting (MRIMath). L.E.: Instituto de Salud Carlos III grant PI22/00069. T.L.-J.: an Asociación Española Contra el Cáncer grant. G.R.H.: NIH/NIBIB grant (P41-EB032840-01). J.S.B.-S.: NIH/NCI grants to Case Western Reserve University School of Medicine. J.P.M.: MOU between OSU Radiation Oncology and OSU Center for Biostatistics. R.B.J.: NIH grants. A.W.: MOU between OSU Radiation Oncology and OSU Biomedical Informatics. T.A.C.: grants (PGDX, Pfizer, AstraZeneca, Illumina, NysnoBio); royalties (PGDX); consulting (Illumina, NysnoBio, Pfizer, BMS, Merck, LG Chem); patents (TMB as predictor of immunotherapy response); stock (Griststone Bio, Nysno Bio). A.N.: consulting (Daiichi-Sankyo, NGK, SparkPlug) to his institution; $2,000 as honoraria. M.W.: grants (Apogenix, Merck, Sharp & Dohme, Merck [EMD], Philogen, Quercis); consulting (Adastra, Medac, Merck [EMD], Nerviano Medical Sciences, Novartis); honoraria (Bristol Meyer Squibb, Medac, Merck, Sharp & Dohme); Data Safety Monitoring Board or Advisory Board (Orbus and Philogen); leadership (EORTC). R.G.W.: grant 70-3163-Wi 3 (German Cancer Aid). S.O.: grant (Cordia Therapeutics, Dainippon-Sumitomo, Pharmaceuticals, Otsuka Assay Inc.); royalties (ASAHI Genomics, Qiagen); consulting (Cordia Therapeutics, Kan Research Institute, Novartis Pharmaceuticals); honoraria (MSD Japan, Kyowa Hakko Kirin, Pfizer); stocks (ASAHI Genomics, Cordia Therapeutics, Rebirthell). M.M.: NIH grants (R01NS092597, DP1NS111132, P50CA165962), grants from Kleberg Foundation Cancer Research, Ludwig Fund for Cancer Research; consulting (Cygnal Therapeutics); honoraria for lectures. C.R.M. and F.B.F.: NIH grant (R01CA258248). F.B.F.: NIH grant (R01NS080939). D.R.M.: clinical trials support (INTELLANCE-1 study [M13-813], CCTG CE.8 [EORTC-1709-BTG], INDIGO study [AG-881], Abbvie, Celgene, Agios [now Servier]).

INCLUSION AND DIVERSITY

We worked to ensure gender balance in the recruitment of human subjects, ethnic or other types of diversity in the recruitment of human subjects, that the study questionnaires were prepared in an inclusive way, sex balance in the selection of non-human subjects, diversity in experimental samples through the selection of the cell lines, diversity in experimental samples through the selection of the genomic datasets. Multiple authors self-identify as an underrepresented ethnic minority in their field of research or within their geographical location or a gender minority in their field of research. One or more of the authors of this paper received support from a program designed to increase minority representation in their field of research. While citing

Cell Reports Medicine
Article

references scientifically relevant to this work, we also actively worked to promote gender balance in our reference list.

REFERENCES

1. Eckel-Passow, J.E., Lachance, D.H., Molinaro, A.M., Walsh, K.M., Decker, P.A., Sicotte, H., Pekmezci, M., Rice, T., Kosel, M.L., Smirnov, I.V., et al. (2015). Glioma groups based on 1p/19q, IDH, and TERT promoter mutations in tumors. N. Engl. J. Med. *372*, 2499–2508. https://doi.org/10.1056/NEJMoa1407279.

2. Cancer Genome Atlas Research Network; Brat, D.J., Verhaak, R.G.W., Aldape, K.D., Yung, W.K.A., Salama, S.R., Cooper, L.A.D., Rheinbay, E., Miller, C.R., Vitucci, M., et al. (2015). Comprehensive, integrative genomic analysis of diffuse lower-grade gliomas. N. Engl. J. Med. *372*, 2481–2498. https://doi.org/10.1056/NEJMoa1402121.

3. Suzuki, H., Aoki, K., Chiba, K., Sato, Y., Shiozawa, Y., Shiraishi, Y., Shimamura, T., Niida, A., Motomura, K., Ohka, F., et al. (2015). Mutational landscape and clonal architecture in grade II and III gliomas. Nat. Genet. *47*, 458–468. https://doi.org/10.1038/ng.3273.

4. Ceccarelli, M., Barthel, F.P., Malta, T.M., Sabedot, T.S., Salama, S.R., Murray, B.A., Morozova, O., Newton, Y., Radenbaugh, A., Pagnotta, S.M., et al. (2016). Molecular profiling reveals biologically discrete subsets and pathways of progression in diffuse glioma. Cell *164*, 550–563. https://doi.org/10.1016/j.cell.2015.12.028.

5. Johnson, K.C., Anderson, K.J., Courtois, E.T., Gujar, A.D., Barthel, F.P., Varn, F.S., Luo, D., Seignon, M., Yi, E., Kim, H., et al. (2021). Single-cell multimodal glioma analyses identify epigenetic regulators of cellular plasticity and environmental stress response. Nat. Genet. *53*, 1456–1468. https://doi.org/10.1038/s41588-021-00926-8.

6. Cancer Genome Atlas Research Network (2008). Comprehensive genomic characterization defines human glioblastoma genes and core pathways. Nature *455*, 1061–1068. https://doi.org/10.1038/nature07385.

7. Verhaak, R.G.W., Hoadley, K.A., Purdom, E., Wang, V., Qi, Y., Wilkerson, M.D., Miller, C.R., Ding, L., Golub, T., Mesirov, J.P., et al. (2010). Integrated genomic analysis identifies clinically relevant subtypes of glioblastoma characterized by abnormalities in PDGFRA, IDH1, EGFR, and NF1. Cancer Cell *17*, 98–110. https://doi.org/10.1016/j.ccr.2009.12.020.

8. Yan, H., Parsons, D.W., Jin, G., McLendon, R., Rasheed, B.A., Yuan, W., Kos, I., Batinic-Haberle, I., Jones, S., Riggins, G.J., et al. (2009). IDH1 and IDH2 mutations in gliomas. N. Engl. J. Med. *360*, 765–773. https://doi.org/10.1056/NEJMoa0808710.

9. Killela, P.J., Reitman, Z.J., Jiao, Y., Bettegowda, C., Agrawal, N., Diaz, L.A., Jr., Friedman, A.H., Friedman, H., Gallia, G.L., Giovanella, B.C., et al. (2013). TERT promoter mutations occur frequently in gliomas and a subset of tumors derived from cells with low rates of self-renewal. Proc. Natl. Acad. Sci. USA *110*, 6021–6026. https://doi.org/10.1073/pnas.1303607110.

10. Heaphy, C.M., de Wilde, R.F., Jiao, Y., Klein, A.P., Edil, B.H., Shi, C., Bettegowda, C., Rodriguez, F.J., Eberhart, C.G., Hebbar, S., et al. (2011). Altered telomeres in tumors with ATRX and DAXX mutations. Science *333*, 425. https://doi.org/10.1126/science.1207313.

11. Jenkins, R.B., Blair, H., Ballman, K.V., Giannini, C., Arusell, R.M., Law, M., Flynn, H., Passe, S., Felten, S., Brown, P.D., et al. (2006). A t(1;19)(q10;p10) mediates the combined deletions of 1p and 19q and predicts a better prognosis of patients with oligodendroglioma. Cancer Res. *66*, 9852–9861. https://doi.org/10.1158/0008-5472.CAN-06-1796.

12. Louis, D.N., Perry, A., Wesseling, P., Brat, D.J., Cree, I.A., Figarella-Branger, D., Hawkins, C., Ng, H.K., Pfister, S.M., Reifenberger, G., et al. (2021). The 2021 WHO classification of tumors of the central nervous system: a summary. Neuro Oncol. *23*, 1231–1251. https://doi.org/10.1093/neuonc/noab106.

13. Turcan, S., Rohle, D., Goenka, A., Walsh, L.A., Fang, F., Yilmaz, E., Campos, C., Fabius, A.W.M., Lu, C., Ward, P.S., et al. (2012). IDH1 mutation is sufficient to establish the glioma hypermethylator phenotype. Nature *483*, 479–483. https://doi.org/10.1038/nature10866.

14. Malta, T.M., de Souza, C.F., Sabedot, T.S., Silva, T.C., Mosella, M.S., Kalkanis, S.N., Snyder, J., Castro, A.V.B., and Noushmehr, H. (2018). Glioma CpG island methylator phenotype (G-CIMP): biological and clinical implications. Neuro Oncol. *20*, 608–620. https://doi.org/10.1093/neuonc/nox183.

15. Noushmehr, H., Weisenberger, D.J., Diefes, K., Phillips, H.S., Pujara, K., Berman, B.P., Pan, F., Pelloski, C.E., Sulman, E.P., Bhat, K.P., et al. (2010). Identification of a CpG island methylator phenotype that defines a distinct subgroup of glioma. Cancer Cell *17*, 510–522. https://doi.org/10.1016/j.ccr.2010.03.017.

16. de Souza, C.F., Sabedot, T.S., Malta, T.M., Stetson, L., Morozova, O., Sokolov, A., Laird, P.W., Wiznerowicz, M., Iavarone, A., Snyder, J., et al. (2018). A distinct DNA methylation shift in a subset of glioma CpG island methylator phenotypes during tumor recurrence. Cell Rep. *23*, 637–651. https://doi.org/10.1016/j.celrep.2018.03.107.

17. Nagaraja, S., Quezada, M.A., Gillespie, S.M., Arzt, M., Lennon, J.J., Woo, P.J., Hovestadt, V., Kambhampati, M., Filbin, M.G., Suva, M.L., et al. (2019). Histone variant and cell context determine H3K27M reprogramming of the enhancer landscape and oncogenic state. Mol. Cell *76*, 965–980.e12. https://doi.org/10.1016/j.molcel.2019.08.030.

18. Schwartzentruber, J., Korshunov, A., Liu, X.Y., Jones, D.T.W., Pfaff, E., Jacob, K., Sturm, D., Fontebasso, A.M., Quang, D.A.K., Tönjes, M., et al. (2012). Driver mutations in histone H3.3 and chromatin remodelling genes in paediatric glioblastoma. Nature *482*, 226–231. https://doi.org/10.1038/nature10833.

19. Wu, G., Diaz, A.K., Paugh, B.S., Rankin, S.L., Ju, B., Li, Y., Zhu, X., Qu, C., Chen, X., Zhang, J., et al. (2014). The genomic landscape of diffuse intrinsic pontine glioma and pediatric non-brainstem high-grade glioma. Nat. Genet. *46*, 444–450. https://doi.org/10.1038/ng.2938.

20. Lewis, P.W., Müller, M.M., Koletsky, M.S., Cordero, F., Lin, S., Banaszynski, L.A., Garcia, B.A., Muir, T.W., Becher, O.J., and Allis, C.D. (2013). Inhibition of PRC2 activity by a gain-of-function H3 mutation found in pediatric glioblastoma. Science *340*, 857–861. https://doi.org/10.1126/science.1232245.

21. Bender, S., Tang, Y., Lindroth, A.M., Hovestadt, V., Jones, D.T.W., Kool, M., Zapatka, M., Northcott, P.A., Sturm, D., Wang, W., et al. (2013). Reduced H3K27me3 and DNA hypomethylation are major drivers of gene expression in K27M mutant pediatric high-grade gliomas. Cancer Cell *24*, 660–672. https://doi.org/10.1016/j.ccr.2013.10.006.

22. Müller, J. (1995). Transcriptional silencing by the Polycomb protein in Drosophila embryos. EMBO J. *14*, 1209–1220. https://doi.org/10.1002/j.1460-2075.1995.tb07104.x.

23. Beg, A.A., Ruben, S.M., Scheinman, R.I., Haskill, S., Rosen, C.A., and Baldwin, A.S. (1992). I kappa B interacts with the nuclear localization sequences of the subunits of NF-kappa B: a mechanism for cytoplasmic retention. Genes Dev. *6*, 1899–1913. https://doi.org/10.1101/gad.6.10.1899.

24. Mulero, M.C., Ferres-Marco, D., Islam, A., Margalef, P., Pecoraro, M., Toll, A., Drechsel, N., Charneco, C., Davis, S., Bellora, N., et al. (2013). Chromatin-bound IκBα regulates a subset of polycomb target genes in differentiation and cancer. Cancer Cell *24*, 151–166. https://doi.org/10.1016/j.ccr.2013.06.003.

25. Marruecos, L., Bertran, J., Álvarez-Villanueva, D., Mulero, M.C., Guillén, Y., Palma, L.G., Floor, M., Vert, A., Arce-Gallego, S., Pecharroman, I., et al. (2021). Dynamic chromatin association of IκBα is regulated by acetylation and cleavage of histone H4. EMBO Rep. *22*, e52649. https://doi.org/10.15252/embr.202152649.

26. Espinosa, L., and Marruecos, L. (2021). NF-κB-Dependent and -independent (moonlighting) IκBα functions in differentiation and cancer. Biomedicines 9, 1278. https://doi.org/10.3390/biomedicines9091278.

27. Bredel, M., Scholtens, D.M., Yadav, A.K., Alvarez, A.A., Renfrow, J.J., Chandler, J.P., Yu, I.L.Y., Carro, M.S., Dai, F., Tagge, M.J., et al. (2011). NFKBIA deletion in glioblastomas. N. Engl. J. Med. 364, 627–637. https://doi.org/10.1056/NEJMoa1006312.

28. Buckner, J.C., Shaw, E.G., Pugh, S.L., Chakravarti, A., Gilbert, M.R., Barger, G.R., Coons, S., Ricci, P., Bullard, D., Brown, P.D., et al. (2016). Radiation plus procarbazine, CCNU, and vincristine in low-grade glioma. N. Engl. J. Med. 374, 1344–1355. https://doi.org/10.1056/NEJMoa1500925.

29. D'Angelo, F., Ceccarelli, M., Tala, Garofano, L., Zhang, J., Frattini, V., Caruso, F.P., Lewis, G., Alfaro, K.D., Bauchet, L., et al. (2019). The molecular landscape of glioma in patients with Neurofibromatosis 1. Nat. Med. 25, 176–187. https://doi.org/10.1038/s41591-018-0263-8.

30. Meissner, A., Mikkelsen, T.S., Gu, H., Wernig, M., Hanna, J., Sivachenko, A., Zhang, X., Bernstein, B.E., Nusbaum, C., Jaffe, D.B., et al. (2008). Genome-scale DNA methylation maps of pluripotent and differentiated cells. Nature 454, 766–770. https://doi.org/10.1038/nature07107.

31. Estève, P.O., Chin, H.G., Smallwood, A., Feehery, G.R., Gangisetty, O., Karpf, A.R., Carey, M.F., and Pradhan, S. (2006). Direct interaction between DNMT1 and G9a coordinates DNA and histone methylation during replication. Genes Dev. 20, 3089–3103. https://doi.org/10.1101/gad.1463706.

32. Allis, C.D., and Jenuwein, T. (2016). The molecular hallmarks of epigenetic control. Nat. Rev. Genet. 17, 487–500. https://doi.org/10.1038/nrg.2016.59.

33. Dixit, D., Prager, B.C., Gimple, R.C., Miller, T.E., Wu, Q., Yomtoubian, S., Kidwell, R.L., Lv, D., Zhao, L., Qiu, Z., et al. (2022). Glioblastoma stem cells reprogram chromatin in vivo to generate selective therapeutic dependencies on DPY30 and phosphodiesterases. Sci. Transl. Med. 14, eabf3917. https://doi.org/10.1126/scitranslmed.abf3917.

34. Xu, W., Yang, H., Liu, Y., Yang, Y., Wang, P., Kim, S.H., Ito, S., Yang, C., Wang, P., Xiao, M.T., et al. (2011). Oncometabolite 2-hydroxyglutarate is a competitive inhibitor of α-ketoglutarate-dependent dioxygenases. Cancer Cell 19, 17–30. https://doi.org/10.1016/j.ccr.2010.12.014.

35. Viswanath, P., Najac, C., Izquierdo-Garcia, J.L., Pankov, A., Hong, C., Eriksson, P., Costello, J.F., Pieper, R.O., and Ronen, S.M. (2016). Mutant IDH1 expression is associated with down-regulation of monocarboxylate transporters. Oncotarget 7, 34942–34955. https://doi.org/10.18632/oncotarget.9006.

36. Cai, Y., Zhang, Y., Loh, Y.P., Tng, J.Q., Lim, M.C., Cao, Z., Raju, A., Lieberman Aiden, E., Li, S., Manikandan, L., et al. (2021). H3K27me3-rich genomic regions can function as silencers to repress gene expression via chromatin interactions. Nat. Commun. 12, 719. https://doi.org/10.1038/s41467-021-20940-y.

37. Healy, E., Mucha, M., Glancy, E., Fitzpatrick, D.J., Conway, E., Neikes, H.K., Monger, C., Van Mierlo, G., Baltissen, M.P., Koseki, Y., et al. (2019). PRC2.1 and PRC2.2 synergize to coordinate H3K27 trimethylation. Mol. Cell 76, 437–452.e6. https://doi.org/10.1016/j.molcel.2019.08.012.

38. Loh, C.H., van Genesen, S., Perino, M., Bark, M.R., and Veenstra, G.J.C. (2021). Loss of PRC2 subunits primes lineage choice during exit of pluripotency. Nat. Commun. 12, 6985. https://doi.org/10.1038/s41467-021-27314-4.

39. Gray, F., Cho, H.J., Shukla, S., He, S., Harris, A., Boytsov, B., Jaremko, Ł., Jaremko, M., Demeler, B., Lawlor, E.R., et al. (2016). BMI1 regulates PRC1 architecture and activity through homo- and hetero-oligomerization. Nat. Commun. 7, 13343. https://doi.org/10.1038/ncomms13343.

40. Wang, H., Wang, L., Erdjument-Bromage, H., Vidal, M., Tempst, P., Jones, R.S., and Zhang, Y. (2004). Role of histone H2A ubiquitination in Polycomb silencing. Nature 431, 873–878. https://doi.org/10.1038/nature02985.

41. Feng, G., and Sun, Y. (2022). The Polycomb group gene. Front. Neurosci. 16, 960149. https://doi.org/10.3389/fnins.2022.960149.

42. Dang, L., White, D.W., Gross, S., Bennett, B.D., Bittinger, M.A., Driggers, E.M., Fantin, V.R., Jang, H.G., Jin, S., Keenan, M.C., et al. (2010). Cancer-associated IDH1 mutations produce 2-hydroxyglutarate. Nature 465, 966. https://doi.org/10.1038/nature09132.

43. Chung, C., Sweha, S.R., Pratt, D., Tamrazi, B., Panwalkar, P., Banda, A., Bayliss, J., Hawes, D., Yang, F., Lee, H.J., et al. (2020). Integrated metabolic and epigenomic reprograming by H3K27M mutations in diffuse intrinsic pontine gliomas. Cancer Cell 38, 334–349.e9. https://doi.org/10.1016/j.ccell.2020.07.008.

44. Bhat, K.P.L., Balasubramaniyan, V., Vaillant, B., Ezhilarasan, R., Hummelink, K., Hollingsworth, F., Wani, K., Heathcock, L., James, J.D., Goodman, L.D., et al. (2013). Mesenchymal differentiation mediated by NF-κB promotes radiation resistance in glioblastoma. Cancer Cell 24, 331–346. https://doi.org/10.1016/j.ccr.2013.08.001.

45. Soubannier, V., and Stifani, S. (2017). NF-κB signalling in glioblastoma. Biomedicines 5, 29. https://doi.org/10.3390/biomedicines5020029.

46. Harutyunyan, A.S., Krug, B., Chen, H., Papillon-Cavanagh, S., Zeinieh, M., De Jay, N., Deshmukh, S., Chen, C.C.L., Belle, J., Mikael, L.G., et al. (2019). H3K27M induces defective chromatin spread of PRC2-mediated repressive H3K27me2/me3 and is essential for glioma tumorigenesis. Nat. Commun. 10, 1262. https://doi.org/10.1038/s41467-019-09140-x.

47. Højfeldt, J.W., Laugesen, A., Willumsen, B.M., Damhofer, H., Hedehus, L., Tvardovskiy, A., Mohammad, F., Jensen, O.N., and Helin, K. (2018). Accurate H3K27 methylation can be established de novo by SUZ12-directed PRC2. Nat. Struct. Mol. Biol. 25, 225–232. https://doi.org/10.1038/s41594-018-0036-6.

48. Cao, R., Wang, L., Wang, H., Xia, L., Erdjument-Bromage, H., Tempst, P., Jones, R.S., and Zhang, Y. (2002). Role of histone H3 lysine 27 methylation in Polycomb-group silencing. Science 298, 1039–1043. https://doi.org/10.1126/science.1076997.

49. Lu, C., Ward, P.S., Kapoor, G.S., Rohle, D., Turcan, S., Abdel-Wahab, O., Edwards, C.R., Khanin, R., Figueroa, M.E., Melnick, A., et al. (2012). IDH mutation impairs histone demethylation and results in a block to cell differentiation. Nature 483, 474–478. https://doi.org/10.1038/nature10860.

50. Harutyunyan, A.S., Chen, H., Lu, T., Horth, C., Nikbakht, H., Krug, B., Russo, C., Bareke, E., Marchione, D.M., Coradin, M., et al. (2020). H3K27M in gliomas causes a one-step decrease in H3K27 methylation and reduced spreading within the constraints of H3K36 methylation. Cell Rep. 33, 108390. https://doi.org/10.1016/j.celrep.2020.108390.

51. Diehl, K.L., Ge, E.J., Weinberg, D.N., Jani, K.S., Allis, C.D., and Muir, T.W. (2019). PRC2 engages a bivalent H3K27M-H3K27me3 dinucleosome inhibitor. Proc. Natl. Acad. Sci. USA 116, 22152–22157. https://doi.org/10.1073/pnas.1911775116.

52. Funato, K., Major, T., Lewis, P.W., Allis, C.D., and Tabar, V. (2014). Use of human embryonic stem cells to model pediatric gliomas with H3.3K27M histone mutation. Science 346, 1529–1533. https://doi.org/10.1126/science.1253799.

53. Filbin, M.G., Tirosh, I., Hovestadt, V., Shaw, M.L., Escalante, L.E., Mathewson, N.D., Neftel, C., Frank, N., Pelton, K., Hebert, C.M., et al. (2018). Developmental and oncogenic programs in H3K27M gliomas dissected by single-cell RNA-seq. Science 360, 331–335. https://doi.org/10.1126/science.aao4750.

54. Castel, D., Philippe, C., Kergrohen, T., Sill, M., Merlevede, J., Barret, E., Puget, S., Sainte-Rose, C., Kramm, C.M., Jones, C., et al. (2018). Transcriptomic and epigenetic profiling of 'diffuse midline gliomas, H3 K27M-mutant' discriminate two subgroups based on the type of histone H3 mutated and not supratentorial or infratentorial location. Acta Neuropathol. Commun. 6, 117. https://doi.org/10.1186/s40478-018-0614-1.

55. Ben-Porath, I., Thomson, M.W., Carey, V.J., Ge, R., Bell, G.W., Regev, A., and Weinberg, R.A. (2008). An embryonic stem cell-like gene

expression signature in poorly differentiated aggressive human tumors. Nat. Genet. *40*, 499–507. https://doi.org/10.1038/ng.127.

56. Fang, D., Gan, H., Cheng, L., Lee, J.H., Zhou, H., Sarkaria, J.N., Daniels, D.J., and Zhang, Z. (2018). H3.3K27M mutant proteins reprogram epigenome by sequestering the PRC2 complex to poised enhancers. Elife *7*, e36696. https://doi.org/10.7554/eLife.36696.

57. Lewis, E.B. (1978). A gene complex controlling segmentation in Drosophila. Nature *276*, 565–570. https://doi.org/10.1038/276565a0.

58. Gentile, C., and Kmita, M. (2020). Polycomb repressive complexes in hox gene regulation: silencing and beyond: the functional dynamics of polycomb repressive complexes in hox gene regulation. Bioessays *42*, e1900249. https://doi.org/10.1002/bies.201900249.

59. Gorlia, T., van den Bent, M.J., Hegi, M.E., Mirimanoff, R.O., Weller, M., Cairncross, J.G., Eisenhauer, E., Belanger, K., Brandes, A.A., Allgeier, A., et al. (2008). Nomograms for predicting survival of patients with newly diagnosed glioblastoma: prognostic factor analysis of EORTC and NCIC trial 26981-22981/CE.3. Lancet Oncol. *9*, 29–38. https://doi.org/10.1016/S1470-2045(07)70384-4.

60. Nomura, M., Saito, K., Aihara, K., Nagae, G., Yamamoto, S., Tatsuno, K., Ueda, H., Fukuda, S., Umeda, T., Tanaka, S., et al. (2019). DNA demethylation is associated with malignant progression of lower-grade gliomas. Sci. Rep. *9*, 1903. https://doi.org/10.1038/s41598-019-38510-0.

61. Chaligne, R., Gaiti, F., Silverbush, D., Schiffman, J.S., Weisman, H.R., Kluegel, L., Gritsch, S., Deochand, S.D., Gonzalez Castro, L.N., Richman, A.R., et al. (2021). Epigenetic encoding, heritability and plasticity of glioma transcriptional cell states. Nat. Genet. *53*, 1469–1479. https://doi.org/10.1038/s41588-021-00927-7.

62. Raineri, S., and Mellor, J. (2018). Linking metabolism and epigenetics. Front. Genet. *9*, 493. https://doi.org/10.3389/fgene.2018.00493.

63. Reddington, J.P., Perricone, S.M., Nestor, C.E., Reichmann, J., Youngson, N.A., Suzuki, M., Reinhardt, D., Dunican, D.S., Prendergast, J.G., Mjoseng, H., et al. (2013). Redistribution of H3K27me3 upon DNA hypomethylation results in de-repression of Polycomb target genes. Genome Biol. *14*, R25. https://doi.org/10.1186/gb-2013-14-3-r25.

64. Brena, D., Bertran, J., Porta-de-la-Riva, M., Guillén, Y., Cornes, E., Kukhtar, D., Campos-Vicens, L., Fernández, L., Pecharroman, I., García-López, A., et al. (2020). Ancestral function of Inhibitors-of-kappaB regulates Caenorhabditis elegans development. Sci. Rep. *10*, 16153. https://doi.org/10.1038/s41598-020-73146-5.

65. Venkatesh, H.S., Morishita, W., Geraghty, A.C., Silverbush, D., Gillespie, S.M., Arzt, M., Tam, L.T., Espenel, C., Ponnuswami, A., Ni, L., et al. (2019). Electrical and synaptic integration of glioma into neural circuits. Nature *573*, 539–545. https://doi.org/10.1038/s41586-019-1563-y.

66. Venkatesh, H.S., Johung, T.B., Caretti, V., Noll, A., Tang, Y., Nagaraja, S., Gibson, E.M., Mount, C.W., Polepalli, J., Mitra, S.S., et al. (2015). Neuronal activity promotes glioma growth through neuroligin-3 secretion. Cell *161*, 803–816. https://doi.org/10.1016/j.cell.2015.04.012.

67. Venkataramani, V., Tanev, D.I., Strahle, C., Studier-Fischer, A., Fankhauser, L., Kessler, T., Körber, C., Kardorff, M., Ratliff, M., Xie, R., et al. (2019). Glutamatergic synaptic input to glioma cells drives brain tumour progression. Nature *573*, 532–538. https://doi.org/10.1038/s41586-019-1564-x.

68. Palomer, E., Carretero, J., Benvegnù, S., Dotti, C.G., and Martin, M.G. (2016). Neuronal activity controls Bdnf expression via Polycomb de-repression and CREB/CBP/JMJD3 activation in mature neurons. Nat. Commun. *7*, 11081. https://doi.org/10.1038/ncomms11081.

69. Natsume, A., Ito, M., Katsushima, K., Ohka, F., Hatanaka, A., Shinjo, K., Sato, S., Takahashi, S., Ishikawa, Y., Takeuchi, I., et al. (2013). Chromatin regulator PRC2 is a key regulator of epigenetic plasticity in glioblastoma. Cancer Res. *73*, 4559–4570. https://doi.org/10.1158/0008-5472.CAN-13-0109.

70. Grasso, C.S., Tang, Y., Truffaux, N., Berlow, N.E., Liu, L., Debily, M.A., Quist, M.J., Davis, L.E., Huang, E.C., Woo, P.J., et al. (2015). Functionally

71. Katagi, H., Louis, N., Unruh, D., Sasaki, T., He, X., Zhang, A., Ma, Q., Piunti, A., Shimazu, Y., Lamano, J.B., et al. (2019). Radiosensitization by histone H3 demethylase inhibition in diffuse intrinsic pontine glioma. Clin. Cancer Res. *25*, 5572–5583. https://doi.org/10.1158/1078-0432.CCR-18-3890.

72. Fang, Y., Liao, G., and Yu, B. (2019). LSD1/KDM1A inhibitors in clinical trials: advances and prospects. J. Hematol. Oncol. *12*, 129. https://doi.org/10.1186/s13045-019-0811-9.

73. Hashizume, R., Andor, N., Ihara, Y., Lerner, R., Gan, H., Chen, X., Fang, D., Huang, X., Tom, M.W., Ngo, V., et al. (2014). Pharmacologic inhibition of histone demethylation as a therapy for pediatric brainstem glioma. Nat. Med. *20*, 1394–1396. https://doi.org/10.1038/nm.3716.

74. Davoli, T., Xu, A.W., Mengwasser, K.E., Sack, L.M., Yoon, J.C., Park, P.J., and Elledge, S.J. (2013). Cumulative haploinsufficiency and triplosensitivity drive aneuploidy patterns and shape the cancer genome. Cell *155*, 948–962. https://doi.org/10.1016/j.cell.2013.10.011.

75. Dichamp, C., Taillibert, S., Aguirre-Cruz, L., Lejeune, J., Marie, Y., Kujas, M., Delattre, J.Y., Hoang-Xuan, K., and Sanson, M. (2004). Loss of 14q chromosome in oligodendroglial and astrocytic tumors. J. Neuro Oncol. *67*, 281–285. https://doi.org/10.1023/b:neon.0000024218.68120.8d.

76. Felsberg, J., Yan, P.S., Huang, T.H.M., Milde, U., Schramm, J., Wiestler, O.D., Reifenberger, G., Pietsch, T., and Waha, A. (2006). DNA methylation and allelic losses on chromosome arm 14q in oligodendroglial tumours. Neuropathol. Appl. Neurobiol. *32*, 517–524. https://doi.org/10.1111/j.1365-2990.2006.00759.x.

77. Hu, J., Pang, J.C.S., Tong, C.Y.K., Lau, B., Yin, X.L., Poon, W.S., Jiang, C.C., Zhou, L.F., and Ng, H.K. (2002). High-resolution genome-wide allelotype analysis identifies loss of chromosome 14q as a recurrent genetic alteration in astrocytic tumours. Br. J. Cancer *87*, 218–224. https://doi.org/10.1038/sj.bjc.6600430.

78. Mazor, T., Pankov, A., Johnson, B.E., Hong, C., Hamilton, E.G., Bell, R.J.A., Smirnov, I.V., Reis, G.F., Phillips, J.J., Barnes, M.J., et al. (2015). DNA methylation and somatic mutations converge on the cell cycle and define similar evolutionary histories in brain tumors. Cancer Cell *28*, 307–317. https://doi.org/10.1016/j.ccell.2015.07.012.

79. Mazor, T., Chesnelong, C., Pankov, A., Jalbert, L.E., Hong, C., Hayes, J., Smirnov, I.V., Marshall, R., Souza, C.F., Shen, Y., et al. (2017). Clonal expansion and epigenetic reprogramming following deletion or amplification of mutant. Proc. Natl. Acad. Sci. USA *114*, 10743–10748. https://doi.org/10.1073/pnas.1708914114.

80. Bai, H., Harmancı, A.S., Erson-Omay, E.Z., Li, J., Coşkun, S., Simon, M., Krischek, B., Özduman, K., Omay, S.B., Sorensen, E.A., et al. (2016). Integrated genomic characterization of IDH1-mutant glioma malignant progression. Nat. Genet. *48*, 59–66. https://doi.org/10.1038/ng.3457.

81. Sonoda, Y., Ozawa, T., Hirose, Y., Aldape, K.D., McMahon, M., Berger, M.S., and Pieper, R.O. (2001). Formation of intracranial tumors by genetically modified human astrocytes defines four pathways critical in the development of human anaplastic astrocytoma. Cancer Res. *61*, 4956–4960.

82. Olshen, A.B., Venkatraman, E.S., Lucito, R., and Wigler, M. (2004). Circular binary segmentation for the analysis of array-based DNA copy number data. Biostatistics *5*, 557–572. https://doi.org/10.1093/biostatistics/kxh008.

83. Zhang, H., Meltzer, P., and Davis, S. (2013). RCircos: an R package for Circos 2D track plots. BMC Bioinformatics *14*, 244. https://doi.org/10.1186/1471-2105-14-244.

84. Aryee, M.J., Jaffe, A.E., Corrada-Bravo, H., Ladd-Acosta, C., Feinberg, A.P., Hansen, K.D., and Irizarry, R.A. (2014). Minfi: a flexible and comprehensive Bioconductor package for the analysis of Infinium DNA methylation microarrays. Bioinformatics *30*, 1363–1369. https://doi.org/10.1093/bioinformatics/btu049.

85. Phipson, B., Maksimovic, J., and Oshlack, A. (2016). missMethyl: an R package for analyzing data from Illumina's HumanMethylation450 platform. Bioinformatics 32, 286–288. https://doi.org/10.1093/bioinformatics/btv560.

86. Collado-Torres, L., Nellore, A., Kammers, K., Ellis, S.E., Taub, M.A., Hansen, K.D., Jaffe, A.E., Langmead, B., and Leek, J.T. (2017). Reproducible RNA-seq analysis using recount2. Nat. Biotechnol. 35, 319–321. https://doi.org/10.1038/nbt.3838.

87. Ritchie, M.E., Phipson, B., Wu, D., Hu, Y., Law, C.W., Shi, W., and Smyth, G.K. (2015). Limma powers differential expression analyses for RNA-sequencing and microarray studies. Nucleic Acids Res. 43, e47. https://doi.org/10.1093/nar/gkv007.

88. Zhang, B., Kirov, S., and Snoddy, J. (2005). WebGestalt: an integrated system for exploring gene sets in various biological contexts. Nucleic Acids Res. 33, W741–W748. https://doi.org/10.1093/nar/gki475.

89. Hulsen, T., de Vlieg, J., and Alkema, W. (2008). BioVenn - a web application for the comparison and visualization of biological lists using area-proportional Venn diagrams. BMC Genom. 9, 488. https://doi.org/10.1186/1471-2164-9-488.

90. Weller, M., Weber, R.G., Willscher, E., Riehmer, V., Hentschel, B., Kreuz, M., Felsberg, J., Beyer, U., Löffler-Wirth, H., Kaulich, K., et al. (2015). Molecular classification of diffuse cerebral WHO grade II/III gliomas using genome- and transcriptome-wide profiling improves stratification of prognostically distinct patient groups. Acta Neuropathol. 129, 679–693. https://doi.org/10.1007/s00401-015-1409-0.

91. Louis, D.N., Perry, A., Reifenberger, G., von Deimling, A., Figarella-Branger, D., Cavenee, W.K., Ohgaki, H., Wiestler, O.D., Kleihues, P., and Ellison, D.W. (2016). The 2016 World Health organization classification of tumors of the central nervous system: a summary. Acta Neuropathol. 131, 803–820. https://doi.org/10.1007/s00401-016-1545-1.

92. Bell, E.H., Zhang, P., Shaw, E.G., Buckner, J.C., Barger, G.R., Bullard, D.E., Mehta, M.P., Gilbert, M.R., Brown, P.D., Stelzer, K.J., et al. (2020). Comprehensive genomic analysis in NRG oncology/RTOG 9802: a Phase III trial of radiation versus radiation plus procarbazine, lomustine (CCNU), and vincristine in high-risk low-grade glioma. J. Clin. Oncol. 38, 3407–3417. https://doi.org/10.1200/JCO.19.02983.

93. Mermel, C.H., Schumacher, S.E., Hill, B., Meyerson, M.L., Beroukhim, R., and Getz, G. (2011). GISTIC2.0 facilitates sensitive and confident localization of the targets of focal somatic copy-number alteration in human cancers. Genome Biol. 12, R41. https://doi.org/10.1186/gb-2011-12-4-r41.

94. Du, P., Zhang, X., Huang, C.C., Jafari, N., Kibbe, W.A., Hou, L., and Lin, S.M. (2010). Comparison of Beta-value and M-value methods for quantifying methylation levels by microarray analysis. BMC Bioinformatics 11, 587. https://doi.org/10.1186/1471-2105-11-587.

95. Benjamini, Y., and Hochberg, Y. (1995). Controlling the false discovery rate: a practical and powerful approach to multiple testing. J. R. Statist. Soc. B 57, 289–300.

96. Bibikova, M., Lin, Z., Zhou, L., Chudin, E., Garcia, E.W., Wu, B., Doucet, D., Thomas, N.J., Wang, Y., Vollmer, E., et al. (2006). High-throughput DNA methylation profiling using universal bead arrays. Genome Res. 16, 383–393. https://doi.org/10.1101/gr.4410706.

97. Kellis, M., Wold, B., Snyder, M.P., Bernstein, B.E., Kundaje, A., Marinov, G.K., Ward, L.D., Birney, E., Crawford, G.E., Dekker, J., et al. (2014). Defining functional DNA elements in the human genome. Proc. Natl. Acad. Sci. USA 111, 6131–6138. https://doi.org/10.1073/pnas.1318948111.

98. Robinson, M.D., and Oshlack, A. (2010). A scaling normalization method for differential expression analysis of RNA-seq data. Genome Biol. 11, R25. https://doi.org/10.1186/gb-2010-11-3-r25.

99. Kim, D., Pertea, G., Trapnell, C., Pimentel, H., Kelley, R., and Salzberg, S.L. (2013). TopHat2: accurate alignment of transcriptomes in the presence of insertions, deletions and gene fusions. Genome Biol. 14, R36. https://doi.org/10.1186/gb-2013-14-4-r36.

100. Liao, Y., Smyth, G.K., and Shi, W. (2014). featureCounts: an efficient general purpose program for assigning sequence reads to genomic features. Bioinformatics 30, 923–930. https://doi.org/10.1093/bioinformatics/btt656.

101. Love, M.I., Huber, W., and Anders, S. (2014). Moderated estimation of fold change and dispersion for RNA-seq data with DESeq2. Genome Biol. 15, 550. https://doi.org/10.1186/s13059-014-0550-8.

102. Renfrow, J.J., Scheck, A.C., Dhawan, N.S., Lukac, P.J., Vogel, H., Chandler, J.P., Raizer, J.J., Harsh, G.R., Chakravarti, A., and Bredel, M. (2011). Gene-protein correlation in single cells. Neuro Oncol. 13, 880–885. https://doi.org/10.1093/neuonc/nor071.

103. Krueger, B., Friedrich, T., Förster, F., Bernhardt, J., Gross, R., and Dandekar, T. (2012). Different evolutionary modifications as a guide to rewire two-component systems. Bioinform. Biol. Insights 6, 97–128. https://doi.org/10.4137/BBI.S9356.

104. Langmead, B., and Salzberg, S.L. (2012). Fast gapped-read alignment with Bowtie 2. Nat. Methods 9, 357–359. https://doi.org/10.1038/nmeth.1923.

105. Zhang, Y., Liu, T., Meyer, C.A., Eeckhoute, J., Johnson, D.S., Bernstein, B.E., Nusbaum, C., Myers, R.M., Brown, M., Li, W., and Liu, X.S. (2008). Model-based analysis of ChIP-seq (MACS). Genome Biol. 9, R137. https://doi.org/10.1186/gb-2008-9-9-r137.

106. Yu, G., Wang, L.G., and He, Q.Y. (2015). ChIPker: an R/Bioconductor package for ChIP peak annotation, comparison and visualization. Bioinformatics 31, 2382–2383. https://doi.org/10.1093/bioinformatics/btv145.

107. Kuleshov, M.V., Jones, M.R., Rouillard, A.D., Fernandez, N.F., Duan, Q., Wang, Z., Koplev, S., Jenkins, S.L., Jagodnik, K.M., Lachmann, A., et al. (2016). Enrichr: a comprehensive gene set enrichment analysis web server 2016 update. Nucleic Acids Res. 44, W90–W97. https://doi.org/10.1093/nar/gkw377.

108. Lachmann, A., Xu, H., Krishnan, J., Berger, S.I., Mazloom, A.R., and Ma'ayan, A. (2010). ChEA: transcription factor regulation inferred from integrating genome-wide ChIP-X experiments. Bioinformatics 26, 2438–2444. https://doi.org/10.1093/bioinformatics/btq466.

109. Clarke, D.J.B., Jeon, M., Stein, D.J., Moiseyev, N., Kropiwnicki, E., Dai, C., Xie, Z., Wojciechowicz, M.L., Litz, S., Hom, J., et al. (2021). Appyters: turning jupyter notebooks into data-driven web apps. Patterns 2, 100213. https://doi.org/10.1016/j.patter.2021.100213.

110. Schemper, M., and Smith, T.L. (1996). A note on quantifying follow-up in studies of failure time. Control. Clin. Trials 17, 343–346. https://doi.org/10.1016/0197-2456(96)00075-x.

111. Heinze, G., Gnant, M., and Schemper, M. (2003). Exact log-rank tests for unequal follow-up. Biometrics 59, 1151–1157. https://doi.org/10.1111/j.0006-341x.2003.00132.x.

112. WOOLF, B. (1955). On estimating the relation between blood group and disease. Ann. Hum. Genet. 19, 251–253. https://doi.org/10.1111/j.1469-1809.1955.tb01348.x.

113. Wahid, A., Khan, D.M., and Hussain, I. (2017). Robust Adaptive Lasso method for parameter's estimation and variable selection in high-dimensional sparse models. PLoS One 12, e0183518. https://doi.org/10.1371/journal.pone.0183518.

114. Chambless, L.E., and Diao, G. (2006). Estimation of time-dependent area under the ROC curve for long-term risk prediction. Stat. Med. 25, 3474–3486. https://doi.org/10.1002/sim.2299.

STAR★METHODS

KEY RESOURCES TABLE

REAGENT or RESOURCE	SOURCE	IDENTIFIER
Antibodies		
Mouse monoclonal IκBα	Cell Signaling Technology	Cat# 4814S; RRID: AB_390781
Mouse monoclonal β-Actin	Cell Signaling Technology	Cat# 3700; RRID: AB_2242334
Rabbit monoclonal Tri-Methyl-Histone H3(Lys27)	Cell Signaling Technology	Cat# 9733S; RRID: AB_2616029
Mouse monoclonal Di/Tri-Methyl-histone H3 (Lys9)	Cell Signaling Technology	Cat# 5327S; RRID: AB_10695295
Mouse monoclonal Anti-5-methylcytosine (5-mC)	Abcam	Cat# ab10805; RRID: AB_442823
Rabbit monoclonal Ezh2	Cell Signaling Technology	Cat# 5246S; RRID: AB_10694683
Mouse monoclonal Anti-IDH1 R132H	Dianova manufacture	Cat# DIA-H09; RRID: AB_2335716
Mouse monoclonal PP1 (E−9)	Santa Cruz	Cat# 7482; RRID: AB_628177
Mouse monoclonal Phospho IκBα	Cell signaling	Cat# 9246; RRID: AB_22267145
Mouse monoclonal Anti-α-Tubulin	Sigma Aldrich	Cat# T6074; RRID:AB_477582
Rabbit monoclonal Anti-Histone H3	Abcam	Cat# ab1791; RRID: AB_302613
Anti-mouse IgG, HRP-linked Antibody	Cell Signaling	Cat# 7076; RRID:AB_330924
Anti-rabbit IgG, HRP-Linked Antibody	Cell Signaling	Cat# 7074; RRID:AB_2099233
Donkey anti-mouse IgG (H + L) Alexa Fluor™ 594	Thermo Fisher/Invitrogen	Cat# R37115; RRID:AB_2556543
Bacterial and virus strains		
Retroviral vector pLNCX2	Turcan et al.[13]	N/A
Biological samples		
Diffuse glioma samples (Populations 1–7)	This study	Table S1
Chemicals, peptides, and recombinant proteins		
Plasmid Transfection Medium	Santa Cruz	Cat# sc-108062
Ultra-Cruz Transfection Reagent	Santa Cruz	Cat# sc-395739
Gibco Geneticin Selective Antibiotic (G418 Sulfate) (50 mg/mL)	Gibco	Cat# 10131-027
TRIzol Reagent	Invitrogen	Cat# 15-596-018
Gibco Opti-MEM I Reduced Serum Medium, no phenol red	Gibco	Cat# 11-058-021
Lipofectamine 2000 Transfection Reagent	Invitrogen	Cat# 11668019
GenomicDNA MiniPrep Kit	Sigma Aldrich	Cat# G1N70-1KT
Critical commercial assays		
TransAM NF-κB Activation Assays │ Colorimetric Kits	Active Motif	Cat# 43296
Nuclear Extract Kit	Active Motif	Cat# 40010
EpiQuik Global Histone H3K27 Methylation Assay Kit	Epigentek	Cat# P-3020-96
D-2-Hydroxyglutarate Assay Kit (Colorimetric)	Abcam	Cat# ab211070
GenElute Genomic DNA miniprep kit	Sigma Aldrich	Cat# GN170
Deposited data		
Clinical, genetic marker data (Populations 1–7)	This study	Table S2
ChIP-sequencing data	This study	GEO accession # GSE222571

(Continued on next page)

Continued

REAGENT or RESOURCE	SOURCE	IDENTIFIER
RNA-sequencing data	This study	portal.gdc.cancer.gov
RNA-sequencing data	This study	GEO accession #GSE223712
RNA-sequencing data	Nagaraja et al.[17]	GEO accession #GSE126319
RNA-sequencing data	Grasso et al.[70]	dbGaP study accession phs000900.v1.p1
DNA methylation data	This study	portal.gdc.cancer.gov
DNA methylation signature raw data – RTOG 9802	This study	Table S6
NFKBIA methylation raw data – RTOG 9802	This study	Table S6
DNA methylation data	De Souza et al.[16]	https://data.mendeley.com/datasets/hx566mwxnm/
DNA methylation data	Mazor et al.[78]	EGAS00001001255
DNA methylation data	Mazor et al.[79]	EGAS00001001854
DNA methylation data	Bai et al.[80]	EGAS00001001588
DNA copy number variation data	This study	portal.gdc.cancer.gov
NFKBIA DNA CNV raw data – RTOG 9802	This study	Table S6
NFKBIA DNA CNV raw data – Mayo	This study	Table S6
DNA copy number variation data	Suzuki et al.[3]	EGAS00001001044
Sequencing data	This study	portal.gdc.cancer.gov
NFKBIA sequencing raw data	This study	https://github.com/SharedExomes/Prim_Recur_Glioma_NFKBIA_exomes
Experimental models: Cell lines		
NHA (Normal human immortalized astrocytes) Parental	Sonoda et al.[81]	N/A
NHA IDH1 WT	Turcan et al.[13]	N/A
NHA IDH1 R132H	Turcan et al.[13]	N/A
NHA IDH1 WT/KO IkBa	This study	N/A
NHA IDH1 R132H Mut/KO IkBa	This study	N/A
Oligonucleotides		
Accell Human NFKBIA siRNA	Dharmacon (Horizon)	Cat# A-004765-13-0020
Accell Non-targeting Control siRNA	Dharmacon (Horizon)	Cat# D-001910-01-20
Primer: SLC16A3 Forward: ACGAAAAGTGGGTTGGTCAG	Invitrogen	Cat# custome
Primer: SLC16A3 Reverse: CCCCAACAGACACAAGACCT	Invitrogen	Cat# custome
Recombinant DNA		
IκB-α Double Nickase Plasmid (h)	Santa Cruz	Cat# sc-400034-NIC
NFKBIA FISH probe	Empire Genomics	Cat# NFKBIA-20-OR
Software and algorithms		
R	The R project for Statistical Computing	https://www.r-project.org/
R package DNAcopy 1.72.3	Olshen et al.[82]	https://bioconductor.org/packages/release/bioc/html/DNAcopy.html
R package conumee 1.9.0	N/A	https://bioconductor.org/packages/release/bioc/html/conumee.html
R package RCircos 1.2.2	Zhang et al.[83]	https://cran.r-project.org/web/packages/RCircos/index.html
R package minifi 1.44.0	Aryee et al.[84]	https://www.bioconductor.org/packages/release/bioc/html/minfi.html
R package TCGAbiolinksGUI 1.23.0	https://www.biorxiv.org/content/10.1101/147496v2.full	https://www.bioconductor.org/packages/release/bioc/html/TCGAbiolinksGUI.html

(Continued on next page)

Continued

REAGENT or RESOURCE	SOURCE	IDENTIFIER
R package MissMethyl 1.32.0	Phipson et al.[85]	https://bioconductor.org/packages/release/bioc/html/missMethyl.html
R package recount2 1.24.1	Collado-Torres et al.[86]	https://bioconductor.org/packages/release/bioc/html/recount.html
R package limma-voom 3.54.2	Ritchie et al.[87]	https://bioconductor.org/packages/release/bioc/html/limma.html
R package WebGestaltR 0.4.5	Zhang et al.[88]	https://cran.r-project.org/web/packages/WebGestaltR/index.html
R package BioVenn 1.13	Hulsen et al.[89]	https://cran.r-project.org/web/packages/BioVenn/index.html
R package hdnom 6.0.1	https://www.biorxiv.org/content/10.1101/065524v1.full.pdf	https://cran.r-project.org/web/packages/hdnom/index.html

RESOURCE AVAILABILITY

Lead contact
Further information and requests for resources and reagents should be directed to and will be fulfilled by the lead contact, Markus Bredel (mbredel@uab.edu).

Materials availability
Gene-modified primary human astrocytes used in this study are available upon request; additionally, the reagents used in this study are available from the lead contact with a completed Materials Transfer Agreement.

Data and code availability
- RNA-sequencing and ChIP-sequencing data have been deposited into the NIH Gene Expression Omnibus (GEO) repository. The accession numbers for the datasets are listed in the key resources table. This manuscript also analyzes existing, publicly available data. The sources and accession numbers for these datasets are listed in the key resources table.
- This paper does not report original code.
- Any additional information required to reanalyze the data reported in the work paper is available from the lead contact upon request.

EXPERIMENTAL MODEL AND SUBJECT DETAILS

Tumor samples and patient populations
Our study utilized seven study populations of patients with diffuse glioma encompassing 2,343 tumors and 2,255 patients. The demographic and disease characteristics of these populations are shown in Table S1, and their clinico-pathologic-genetic details are listed in Table S2. Where appropriate, institutional review board ethics committee approval was obtained. 530 lower-grade—WHO grade 2 and 3—glioma samples profiled as part of The Cancer Genome Atlas (TCGA) Pilot Project (cancergenome.nih.gov/index.asp) constituted Population 1. Gene copy number, gene expression, sequencing, and clinical data for 513, 530, 513, and 525 tumors, respectively, were obtained from the Open Access and Controlled Access Tier of the NIH Genomic Data Commons (GDC) portal (portal.gdc.cancer.gov) of TCGA upon National Human Genome Research Institute (NHGRI) approval. At the time of data retrieval, there was incomplete overlap in the data types available for each sample. Alignment of sample identifiers yielded 516 samples with mutational sequence and gene dosage data, 508 samples with gene dosage and overall survival data, 515 samples with exon expression data and overall survival data, 425 samples with gene dosage and recurrence-free survival data, and 269 samples with complete mutational, gene dosage and overall survival data. Eighty-seven low-grade (WHO grade 2) glioma patients treated as part of NRG Oncology/Radiation Therapy Oncology Group (RTOG) consortium trials 9802 (A Phase III Trial of Radiation Versus Radiation Plus Procarbazine, Lomustine (CCNU), and Vincristine in High-Risk Low-Grade Glioma)[28] constituted Population 2. A unified sample population of 688 lower-grade gliomas from the Mayo Clinic Genome Consortium, a multi-institutional Japanese study consortium,[3] and the German Glioma Network[90] constituted Population 3. A panel of 1,122 WHO grade 2 to 4 glioma samples profiled as part of TCGA and retrieved from the NIH GDC portal comprised Population 4. Gene copy numbers, sequencing, and clinical data were obtained from the NIH GDC portal. At the time of data retrieval, there was incomplete overlap in the data types available for each sample. Alignment of sample identifiers yielded 1,027 samples with gene dosage and overall survival data and 753 samples with gene dosage and recurrence-free survival data. A panel of 473 WHO grade 2 to 4 glioma specimens treated and profiled at Mayo Clinic (Mayo Clinic Genome Consortium) constituted Population 5. A sample population of 180 primary and recurrent tumors from 154 diffuse glioma

cases belonging to 74 patients profiled at Henry Ford Hospital (n = 154 samples) and 13 patients profiled at Case Western University (n = 26 samples) constituted Population 6. All specimens were collected under institutional review board-approved guidelines and classified according to standards set by the World Health Organization (WHO).[91] A central path review was done for RTOG 9802. Written informed consent was obtained from all patients. Specimens were analyzed by a neuropathologist to confirm the histological diagnosis and the presence of vital tumor tissue without excessive contamination by normal brain and tumor necrosis.

Cell lines

Cultures of immortalized primary human astrocytes[81] constitutively expressing wildtype *IDH1* or mutant *IDH1* (R132H), and corresponding parental cells were obtained from Dr. T.A. Chan (Cleveland Clinic) and prepared as previously described.[13] Stable expression of wildtype or mutant *IDH1* was achieved via transduction with retroviral vector pLNCX2 and selection with G418 at 600 μg/mL (Gibco).[13] Parental cells were grown in Dulbecco's Modified Eagle Medium (MT-10-090-CV, Gibco) supplemented with 10% fetal bovine serum (Sigma) and 5% Pen-strep (Corning); *IDH* wildtype and mutant cells were cultured with Geneticin (G418) at 600 μg/mL (Gibco) as the expression of mutant *IDH1* presented as negative selection.

METHOD DETAILS

Mutational analyses

Pan-Cancer Analysis of Whole Genomes (PCAWG) sequences of the International Cancer Genome Consortium (icgc.org) for diffuse gliomas (Population 1) were analyzed for non-synonymous somatic *NFKBIA* mutations and mapped using GenomeViewer and *Homo sapiens* Genome Reference Consortium Human Build 37 (GRCh37). *IDH* mutations and *TERT* and *ATRX* promoter mutations in Population 1 were obtained from the somatic RNA sequencing-based data of the NIH GDC. In Population 2, immunohistochemistry with the mutation-specific monoclonal antibody IDH1-R132H (Dianova) was used to assess for the canonical *IDH1-R132H* mutation as previously reported.[92] To evaluate for noncanonical *IDH1/2* mutations and mutations in *ATRX*, a customized Ion AmpliSeq (Thermo Fisher Scientific) DNA panel was designed and used. Sequence alignment and variant calling were performed using the Ion Suite and Reporter software. *TERT* promoter mutations were assessed by Sanger sequencing based on methods previously described.[1,92] *ATRX* mutations in Population 5 were assessed by immunohistochemistry (denoted by loss of expression; HPA001906, Sigma Aldrich) or by somatic exon sequencing.

Copy number analyses

Estimates of *NFKBIA* deletion and 1p19q codeletion status in 454 patients of Population 1 and 1,090 patients of Population 4 were generated from data from the Open Access and Controlled Access Tier of the NIH Genomic Data Commons (GDC) portal (portal.gdc.cancer.gov) and were based on Affymetrix SNP 6.0 array data using R package DNAcopy to perform a circular binary segmentation (CBS) analysis[82] followed by numeric focal-level CNV calls using GISTIC2.[93] Masked copy number segments, including those containing the *NFKBIA* locus, were based on CBS, except that a filtering step removed the Y chromosome and probe sets that were previously indicated to be associated with frequent germline copy-number variation. The Infinium Human Methylation 450K BeadChip array and R package conumee, available from The Comprehensive R Network (cran.r-project.org), were used to determine copy number variation (CNV) for *NFKBIA* in 87 patients of Population 2 and 154 tumor samples belonging to 74 patients in Population 6. CNV was assessed in 26 samples in Population 6 via whole exome sequencing on an Illumina platform.[16,78–80] CNV calls on the 450K BeadChip array were made using probes for a region spanning *NFKBIA* ± one megabase pair based on log R ratios (LRRs) calculated by dividing the probe intensity of the query sample by a linear combination of reference samples consisting of material from 52 healthy patients with nominally no copy number aberrations. The threshold for calling *NFKBIA* deletions was determined during chromosome 1p19q codeletion calls based on the distribution of segment LRRs and by eye evaluation of the segment scatterplots. The Affymetrix OncoScan Array was used for *NFKBIA* CNV analysis in 40 patients of Population 2 and 227 patients of Population 5. Probe-level LRRs for the *NFKBIA* region of interest (gene ±1 Mbp) were generated using Nexus Copy Number Software (BioDiscovery) and GRCh37. *NFKBIA* CNV for 261 tumors of Population 3 was generated using Affymetrix GeneChip Human Mapping 250K NspI or CytoScan HD arrays. *NFKBIA* CNV was assessed via array-CGH on a spotted genomic DNA microarray with 10,000 large insert clones allowing for an average resolution of better than 0.5 Mb in 136 patients of Population 3 and on an Agilent custom 8 × 60K aCGH array in 305 patients of Population 5 as described.[1,90] Chromosome 1p19q deletions were also determined based on these arrays, except for Population 5, where codeletions were also determined using a clinical fluorescence *in situ* hybridization (FISH) assay.[1,90]

Methylome analyses

Methylation data for the samples of Population 1 were downloaded from the Broad GDAC Firehose data portal (http://gdac.broadinstitute.org/). Differentially represented CpG probes were identified with the t.test function in R and an FDR of <0.001, and those with differences of beta values—the ratio of the methylated probe intensity and the sum of the methylated and unmethylated probe intensities—of >0.15 between *NFKBIA* wildtype and deleted tumors were selected for further analysis. R package RCircos[83] was used to map differentially methylated CpG probes according to genome position. In Populations 2 and 4, the Infinium Human Methylation 450K BeadChip was used for DNA methylome profiling. In Population 2, data were processed using the R package

minifi.[84] Genome annotation was per Genome Reference Consortium Human Build 37 (GRCh37, hg19). Data were Noob-normalized and M-value transformed.[94] Noob was used so newly profiled samples did not need to be processed with previously processed samples. Probes failing in >10% (by Illumina's detection p value) of samples were removed. Samples failing across >10% of probes were removed. SNP-containing probes were removed. Associations between methylation and *NFKBIA* status were tested using the Wilcoxon rank-sum test on methylation data adjusted by study (residuals from the linear model). FDR-adjusted q-values were computed within the probe list, and an FDR of <0.1 and effect in the same direction was considered validated.[95] In Population 4, Infinium Human Methylation 450K BeadChip data from TCGA project were downloaded from the GDC and used for differential DNA methylome analysis in *NFKBIA* deleted vs. non-deleted gliomas. The Beta-value (β) method was used to estimate epigenome-wide methylation levels using the ratio of intensities between methylated and unmethylated alleles.[96] Methylation changes with a mean β (*NFKBIA* deleted tumors) – mean β (*NFKBIA*-wildtype) of >0.15 and an FDR-adjusted p value of <0.001 were deemed significant.

G-CIMP-low vs. G-CIMP-high calls in 87 tumor samples of Population 2 were made using R package TCGAbiolinksGUI.[4,16] 163 methylation probes were used to establish a random forest model with 10-fold cross-validation and >97% accuracy. Analysis of enrichment of cytosine-phosphate-guanine (CpG) sites that are hypomethylated in *NFKBIA* deleted tumors of Population 4 for genes with repressive H3K27me3 marks compared to mid-frontal lobe of normal brain tissue was done using the ENCODE Uniform Processing Pipeline that allows for making uniform peak calls in histone ChiP-sequencing data.[97] MACS2 peak caller was used to identify broader regions of H3K27me3 enrichment (broadPeaks) that pass a Poisson p value threshold of 0.1 (using MACS2's broad peak mode) and gapped/chained regions of enrichment (gappedPeaks) defined as broadPeaks that contain at least one strong narrowPeak (the latter defined as contiguous enrichment that passes a Poisson p value threshold of 0.01). H3K27me3 marks were intersected with a 3-base pair (bp) region to locate the CpGs. The R package missMethyl[85] was used to identify CpG sites in gene promoters across the genome that showed differential DNA methylation and to define functionally related sets of genes.

RNA sequencing analyses

Raw read counts of RNA-seq data for the diffuse gliomas of Population 1 and Population 4 profiled as part of TCGA were downloaded using R package recount2.[86] Very low expressed genes across samples were filtered out. More specifically, genes were kept when their count-per-million (CPM) values were larger than 1.0 for at least three samples among all samples, which resulted in 27,319 genes. The filtered count matrix was normalized by the trimmed mean of M-values (TMM) method.[98] Differentially expressed genes between two groups (i.e., *NFKBIA* wildtype vs. *NFKBIA* deleted samples) were identified by R package limma-voom[87] with an FDR of 0.05.

Primary RNA-seq data from eleven *H3K27M* mutant diffuse intrinsic pontine gliomas (DIPGs), five H3K27 wildtype DIPGs, and three normal pontine tissue samples in Population 7 were obtained from Nagaraja et al.,[17] Grasso et al.,[70] or generated for this study. For the newly generated data, RNA was extracted from approximately 50 mg of tissue frozen at autopsy. RNA was extracted using the RNeasy Mini Plus Kit (Qiagen), and RNA quality was confirmed using an Agilent Bioanalyzer 2100. Following RNA extraction, sequencing libraries were prepared as described by Nagaraja et al.[17] and sequenced on a NextSeq 500 by the Stanford Functional Genomics Facility. RNA-seq data from two biological replicates (3k3 and 3k16) of human pluripotent stem cell (hPSC) derived oligodendrocyte precursor cells (OPCs) with inducible *H3K27M* expression was obtained from Nagaraja et al.[17] For all RNA-seq analyses, sequencing adaptors were first trimmed using cutadapt (version 1.11), and reads were aligned to the hg19 reference genome using tophat2 version 2.11.[99] Raw counts were obtained by assigning mapped reads to RefSeq genes using Rsubread featureCounts.[100] Using the gene-level counts from the primary data, differential expression analysis was performed using DESeq2 with default settings and a Benjamini-Hochberg FDR threshold of 0.1.[101] For the hPSC-derived oligodencrocyte progentior cell (OPC) dataset, gene-level counts were first converted to transcript per million (TPM). Genes upregulated in cells with induced *H3K27M* expression were defined as features with a TPM log2 fold-change greater than one relative to their *H3K27* wildtype OPC counterparts across both biological replicates.

Functional enrichment analysis of differentially expressed genes was done using the Over-Representation Analysis (ORA) module via R package WebGestaltR.[88] Enriched gene sets were post-processed for redundancy reduction by the weighted set cover function. R package BioVenn was used to graph area-proportional Euler diagrams for the intersection of various gene sets.

Fluorescence *in situ* hybridization (FISH)

FISH was done as described by Renfrow et al.[102] and an *NFKBIA*-specific probe (NFKBIA-20-OR) from Empire Genomics. Briefly, paraffin-embedded slides were deparaffinized starting in xylene, followed by 100% ethanol. Slides were placed in a 10 mM citrate acid solution and microwaved for 5 min. Samples were digested in a pepsin solution at 37°C for 40 min, followed by washing in 70% ethanol for 1 min, 85% ethanol for 1 min, and 100% ethanol for 10 min. Slides were dried on a slide warmer. FISH probes targeting *NFKBIA* (Empire Genomics) were applied per manufacturer instructions, and coverslips were applied and sealed with rubber cement. Probes were denatured at 72°C for 3 min and left to hybridize overnight at 37°C in a dark humidity chamber. The next day slides were washed in 2X SSC (saline sodium citrate) 0.5% tween at 42°C for 2 min, followed by 2X SSC at room temperature for 1 min. After air drying in the dark, VECTASHIELD with DAPI (Vector Laboratories) mounting media and a coverslip prepared the specimen for viewing. Pictures were taken using appropriate fluorescent filters on a Zeiss AXIO Observer D1 microscope. There was no centromere control available as chromosome 14 is acrocentric. We used the criteria that at least 80% of the cells needed to be missing one *NFKBIA* signal to be classified as a hemizygous loss.

Immunofluorescence

Paraffin-embedded slides were placed in two washes of xylene followed by decreasing alcohol content washes and then rehydrated in water. Slides were then placed in an antigen retrieval citrate pH 6.0 solution and microwaved for 5 min. After cooling, slides were washed in TBS and permeabilized in TBS with 0.1% Triton X-100 for 10 min. Slides were then washed in TBS twice for 5 min each. A 1% BSA in TBS with 0.1% Tween 20 blocking buffer was applied for 1 h at 37°C. Primary antibody for NFKBIA (Cat 4814, Cell Signaling) at 1:100 dilution was added and incubated at 4°C overnight. Slides were washed in TBS-T twice for 5 min. A donkey anti-mouse594 secondary antibody (Cat R37115, Thermo Fisher) was then added at a 1:1,000 dilution for 1 h at 37°C in dark conditions. Slides were repeatedly washed with TBS-T twice for 5 min each. VECTASHIELD with DAPI (Vector Laboratories) mounting media and a coverslip prepared the specimen for viewing. Pictures were taken using appropriate fluorescent filters on a Zeiss AXIO Observer D1 microscope.

Knockdown and knockout of *NFKBIA*

For near-complete knockdown of *NFKBIA*, G418-resistant primary human astrocytes transduced to stably express wildtype *IDH1* or mutant *IDH1-(R132H)* were transfected with Accell human NFKBIA small interfering (si)RNA or non-targeting control siRNA (Dharmacon), at 20nM concentration using lipofectamine 2000 reagent (Invitrogen) at 1:1 ratio for 48 h. For complete clustered regularly interspaced short palindromic repeats (CRISPR) knockout of *NFKBIA*, astrocytes were transfected with IκBα Double Nickase Plasmid (h) (sc-400034-NIC, Santa Cruz)—consisting of a pair of plasmids each encoding a D10A mutated Cas9 nuclease and a target-specific 20-nucleotide (nt) guide RNA (gRNA)—using plasmid transfection medium (sc-108062) and Ultra-Cruz transfection reagent (sc-395739) at 1:1.5 ratio and were incubated for 72 h. After incubation, cells were screened for GFP-positivity to select for successfully transfected cells. Cells were then sorted and selected into single cells in a 96-well plate with standard growth medium containing G418 at 0.5 μg/mL as a selection agent to complete screening for successfully transfected cells. Clonally selected cells were expanded into bigger plates. Knockdown and knockout efficiency were assayed by immunoblotting.

mRNA extraction and quantitative polymerase chain reaction (PCR)

Total RNA was extracted from immortalized astrocytes expressing various combinations of wildtype and mutant *IDH1* with or without *NFKBIA* knockdown using TRIzol (Thermo Fisher). To assess mRNA expression levels, 1 μg of total RNA was reverse-transcribed and analyzed by quantitative polymerase chain reaction (qPCR). Reactions for each sample were performed in triplicate using a PCR protocol (95°C activation for 10 min followed by 40 cycles of 95°C for 15 s and 60°C for 1 min) in an ABI StepOnePlus Detection System (Applied Biosystems).

Protein extraction and immunoblotting

Primary human astrocytes were grown to 70% confluency overnight. Whole cell lysate was collected in RIPA buffer containing protease inhibitor, and protein estimation was done using the BCA Assay. Primary antibodies used were NFKBIA/IκBα (ab 4814, Cell Signaling), IDH1-R132H (ab DIA-H09, Dianova), β-Actin (ab 3700, Cell Signaling). Secondary IgG-conjugated horseradish peroxidase (Cell Signaling) was followed by enhanced chemiluminescent (ECL) detection (Thermo Fisher). For the assessment of nuclear phosphorylated-sumoylated NFKBIA (ps-NFKBIA), for cell fractionation, cells were lysed with buffer A (10mM HEPES, 1.5mM MgCl2, 10mM KCl, 0.5mM DTT, 0.05% NP40 (or 0.05% Igepal or Tergitol)) pH 7.9, protease inhibitor cocktail, 4mM N-Ethylmaleimide (NEM) (Sigma, Ref. E3876) (sumoylases inhibitor), in PBS for 20 min on ice and centrifuged at 4°C at 1,000 rcf for 10 min. Supernatants were recovered as the cytoplasmic fraction. 6X Laemmli buffer (SDS–PAGE buffer plus β-mercaptoethanol (Sigma, Ref. M−3148])) was added to the supernatant and sonicated. Pellets were washed with buffer A, centrifuged at 4°C at 1,000 rcf for 10 min, and re-suspended with RIPA buffer on ice (181mL H2O, 2mL DOC 10%, 2mL 1M Tris-HCl pH 8.0, 5.6mL 5M NaCl, 2mL Triton X-100 100% from Merck, 2mL SDS 10%, 400μL 500mM EDTA pH 8.0, 250μL 200mM EGTA, 4mL of 1M β-Glycerol-phosphate, 200μL of 100mM NaOrtovanadate, 500μL 4M NaButyrate), and then sonicated and centrifuged at 13,000 rcf for 10 min at 4°C. Supernatants were recovered as the nuclear fraction, and 1X Laemmli buffer was added. Lysates were analyzed by western blotting using standard SDS–polyacrylamide gel electrophoresis (SDS–PAGE) techniques. In brief, protein samples were boiled in Laemmli buffer for 10 min, run in polyacrylamide gels, and transferred onto polyvinylidene–difluoride (PVDF) membranes (Millipore Ref. IPVH00010). Membranes were incubated overnight at 4°C with the appropriate primary antibodies (anti-Phospho-IkBa (Ser32/36) (5A5) (Cell Signaling, ref. 9246); anti-α-Tubulin (clone B-5-1-2) (Sigma-Aldrich, Ref. T6074); anti-Histone H3 (Abcam, Ref. ab1791); anti-PP1 E−9 (Santa Cruz, Ref. sc-7482), extensively washed, and then incubated with specific secondary horseradish peroxidase-linked antibodies from Dako (Ref. P0260 and P0448). Peroxidase activity was visualized using the enhanced chemiluminescence reagent (Biological Industries ref. 20-500-120) and autoradiography films (GE Healthcare ref. 28906835).

Genomic DNA preparation

Genomic DNA from primary human astrocytes was isolated using the GenElute Mammalian Genomic DNA Miniprep Kit (Sigma Aldrich) and quantified via spectrophotometry.

Global histone methylation analysis

The EpiQuik Global H3-K27 Methylation Assay Kit (EpiGentek) was used per manufacturer's instructions to measure global histone H3-K27 methylation across cultured primary human astrocytes expressing wildtype *IDH1* or mutant *IDH1* with or without knock-down/knockout of *NFKBIA*.

Chromatin immunoprecipitation (ChIP)

After transfection with siRNA targeting *NFKBIA* or a scrambled control, primary human astrocytes were fixed with 37% formalde-hyde, and nuclei were prepared. Samples were sonicated, and DNA was measured using a NanoDrop (Thermo Scientific). Two units of DNA were immunoprecipitated with 5-methylcytosine (10805, Abcam), H3K27me3 (9733S, Cell Signaling), H3K9me3 (5327S, Cell Signaling), IκBα (4814S), or EZH2 (5246S, all Cell Signaling). After DNA recovery, results were evaluated by quantitative PCR using Fast SYBR Green master mix (Applied Biosystem) of the histone mark for the G-CIMP gene *SLC16A3* (ACGAAAAGTGG GTTGGTCAG/CCCCAACAGACACAAGACCT).

ChIP sequencing

Control or *NFKBIA*-depleted primary human astrocytes were incubated and crosslinked with 37% formaldehyde and processed ac-cording to the above ChIP protocol. For immunoprecipitation, a Tri-Methyl-Histone H3 (Lys27) H3K27me3 antibody (9733S, Cell Signaling) was used at 1:50 dilution overnight at 4°C to elute the ChIP DNA samples. DNA samples were sequenced using an Illumina HiSeq 4000 platform. Raw paired-end sequences were filtered by quality (Q > 30) and length (length >20 bp) with Trim Galore.[103] Total filtered sequences were aligned against the reference genome (hg38) with Bowtie2.[104] MACS2 software[105] was run for each replicate considering unique alignments (q-value <0.1). Peak annotation was performed using the ChIPker package.[106]

Transcription factor DNA-binding site analysis

Transcription factor binding site analysis for genes mapping into regions of super-silencers (H3K27me3-rich genomic regions, MRRs) in *NFKBIA* depleted primary immortalized astrocytes was done in EnrichR[107] based on ChIP-X data curated in ChIP Enrichment Anal-ysis (ChEA).[108] A scatterplot of all terms in the ChEA_2022 gene set library was visualized via Appyter.[109] Term frequency-inverse document frequency (TF-IDF) values were computed for the gene set corresponding to each term, and Uniform Mani-fold Approx-imation and Projection (UMAP) was applied to the resulting values for dimension reduction. Terms were plotted based on the first two UMAP dimensions.

D-2-hydroxyglutarate assay

IDH1 mutant or wildtype primary human astrocytes transfected with siRNA or CRISPR targeting *NFKBIA* or scrambled control were seeded in 150 mm dishes at a 1×10^7 cells/well density. A colorimetric enzymatic assay (ab211070, Abcam) was used to assess D-2-Hydroxyglutarate (D-2HG) levels according to the manufacturer's instructions. Samples were spin-filtered using a 10kD spin column for deproteinization to reduce high background. Briefly, 20 μL of each cell lysate were transferred onto 96-well plates in triplicate, and 5 μL of 1 mM D-2HG internal standards were added to each sample well. A freshly prepared reaction mix containing D-2HG assay buffer, D-2HG enzyme, and D-2HG substrate mix was added to each well. Reaction mixes with the cell lysates were incubated for 60 min at 37°C. The samples' optical density (OD) was analyzed at 450 nm using a plate reader. D-2HG concentrations were con-verted to nmol/μL. Experiments were performed in triplicate.

NF-κB family protein activation assay

Nuclear extracts from *IDH1* mutant or wildtype primary human astrocytes transfected with siRNA or CRISPR targeting *NFKBIA* or scrambled control were prepared using an Active Motif Nuclear Extract Kit (40010, Active Motif) according to the manufacturer's protocol. Nucleotide-binding of nuclear NF-κB proteins p65, p50, c-Rel, and RelB was quantified via DNA-binding ELISAs (TransAM NF-κB Family Kit, Active Motif) according to the manufacturer's protocol. 10 μg of nuclear extracts were added to a 96-well plate pre-coated with complete binding buffer. For positive control, 5 μg Raji nuclear extract was used. Activated p65, p50, c-Rel, and RelB nucleotide binding was detected by secondary antibodies conjugated to HRP. Sample absorbance was read at 450 nm using a plate reader. Experiments were performed in triplicate.

QUANTIFICATION AND STATISTICAL ANALYSIS

Unless otherwise specified, all statistical calculations were performed using R software and packages from Bioconductor (www.bioconductor.org/). Median duration of follow-up was calculated with the reverse Kaplan-Meier method.[110] Survival curves were esti-mated with the Kaplan-Meier method, and survival distributions were compared across groups with the log rank test. We also used the Cox proportional-hazards model likelihood-ratio test to test the significance of Kaplan-Meier survival estimate separations and to avoid overestimating significance when the number of samples in each group is not balanced (low variant frequency of the *NFKBIA* deletion).[111] The assumption of proportional hazards was tested using interactions of the predictor variables with time. Estimation of the hazard ratios (HRs) and 95%-confidence (CI) intervals used the Cox regression method. A Cox regression model with likelihood-ratio tests was computed in NRG Oncology/RTOG 9802 with age, *NFKBIA* deletion status, adjuvant therapy randomization

(combined chemoradiation vs. radiation alone), and the interaction between *NFKBIA* and adjuvant treatment as covariates. ANOVA was then applied to this model to obtain the overall p value for effects with more than two levels (e.g., the interaction effect). We performed unadjusted and multivariate Cox proportional-hazards regression analyses for overall survival and recurrence-free survival (time from initial diagnosis to death and tumor recurrence, respectively), adjusting for *NFKBIA* and other genetic and clinicopathologic factors. All categorical variables were treated as nominal categorical variables. During the model-building process, we used alterations of gene dosage (wildtype vs. deleted *NFKBIA* or *CDKN2A/B*, wildtype vs. codeleted chromosome 1p19q, amplified or non-amplified *EGFR*, and presence or absence of chromosome 7 gain/10 loss) or *IDH1/2*, *TERT*, *ATRX*, *TP53*, and *PTEN* status (wildtype vs. mutant) as binary predictors to allow for results that are easier to interpret.

Wilcoxon rank-sum test, *t*-tests, and multiple-comparison one-way ANOVA with post hoc Tukey's test were used to analyze between-group differences for continuous variables and *rxc* contingency-table analysis based on McNemar's test with continuity correction on paired nominal data and Fisher's exact test otherwise. We computed odds ratios (ORs) in contingency-table analyses according to the equation $(a/b)/(c/d)$ using Woolf's method for variance estimation,[112] and CIs for estimated parameters were computed for 'constant chi-square boundaries.' Cramér's V was used as a post-test to estimate effect size in contingency tables with more than 1° of freedom. Standardized residuals for contingency table cells were calculated as the ratio of the difference between the observed count and the expected count to the standard deviation of the expected count. In association studies between *NFKBIA* deletions and patient age, we dichotomized age at 40 ($\leq$40 vs. >40) as this cutoff has been used to define low vs. high-risk disease in low(er)-grade gliomas.[28] The Benjamini-Hochberg procedure was used in multiple testing to control the false-discover rate (FDR).[95]

Nomograms for penalized Cox models were developed based on the R package hdnom. Sparse high-dimensional models were built using an adaptive least absolute shrinkage and selection operator (adaLASSO) with a two-step estimation procedure for automatic variable selection[113] among the covariates *NFKBIA* deletion, *TERT* and *ATRX* mutations, 1p19q codeletion, WHO grade, and patient age (and *CDKN2A/B* deletion and *TP53* mutation in a select model). Built models were internally validated and calibrated using repeated 5-fold cross-validation and performance assessed by time-dependent area under the receiver operating curves (ROC) (t-AUC) proposed by Chambless & Diao.[114] For each round of cross-validation, the data were randomly separated into five groups of equal size, according to package defaults in hdnom. Each of the five groups was used for model validation after parameter estimation based on the other four groups within each distinct round of cross-validation. Models generated in the *IDH* mutant WHO grade 2 to 4 tumors of Population 4 were externally validated and calibrated in the *IDH* mutant WHO grade 2 to 4 tumors of Population 5 as an independent dataset with the same variables, as well as in the pooled lower-grade gliomas of Populations 1 and 5.